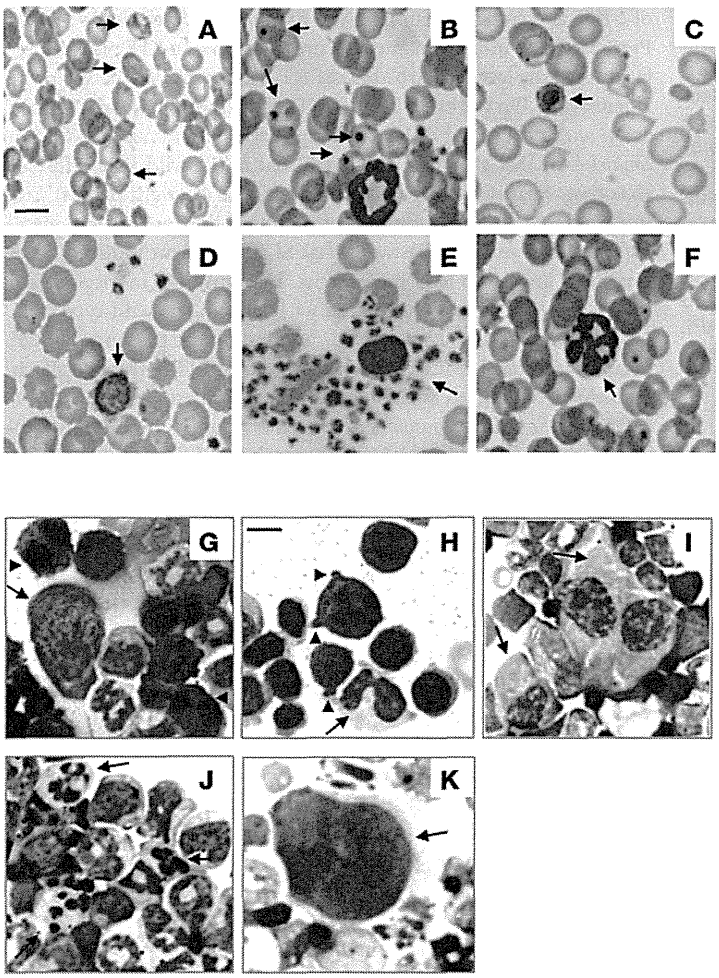


**Figure 6**
Morphology of peripheral blood and bone marrow cells from *Smap1*$^{-/-}$ mice. Smear samples were stained by May-Grunwald Giemsa. (**A–F**) In peripheral blood (PB), the cells are (**A**) polychromatic erythrocytes (arrows), (**B**) Howell-Jolly bodies (arrows), (**C**) erythroblasts (arrows), (**D**) giant platelets (arrow), (**E**) micromegakaryocytes (arrow), and (**F**) hypersegmented neutrophils (arrow). (**G–K**) In bone marrow cells (BM), the abnormal cells include (**G**) megaloblasts (arrow) and binucleated basophilic erythroblasts (arrowheads), (**H**) basophilic erythroblasts with cytoplasmic blebs (arrowheads) and pseudo-Pelger-Huet neutrophils (arrow), (**I**) multinucleated polychromatic megaloblasts, (**J**) orthochromatic erythroblasts with fragmented nuclei (arrows), and (**K**) megakaryocytes with hypolobulated nuclei. Scale bar: 10 μm.

vations suggest a possible involvement of SMAP1 in the MVB-to-lysosome transport pathway.

To verify this, the fate of internalized c-KIT was monitored in relation to Hrs (Figure 5C). After 10 minutes of SCF stimulation, a substantial proportion of internalized c-KIT was colocalized with Hrs, indicating the localization of c-KIT in MVBs. After 20 and 30 minutes, c-KIT colocalization with Hrs was not detected in wild-type MEFs but was present in *Smap1*$^{-/-}$ MEFs, indicating that the transport of c-KIT from the MVB to the lysosome was impaired in *Smap1*-targeted MEFs and possibly explaining the accumulation of internalized c-KIT in *Smap1*$^{-/-}$ BMMCs. The delay in the exit of c-KIT from late endosomes/MVBs in *Smap1*$^{-/-}$ MEFs was confirmed by another marker, Rab7 (Supplemental Figure 2A). However, the exit of c-KIT from early endosomes was not affected by *SMAP1* targeting, as shown by its colocalization with the early endosome marker Rab5 (Supplemental Figure 2B).

The possible involvement of ARF GTPase itself in the intracellular transport of c-KIT was examined in COS7 cells. Overexpression of the active form of ARF, which can mimic *SMAP1* deficiency, induced the substantial colocalization of c-KIT, Hrs, and ARF (Supplemental Figure 3). This implies the delay or block of c-KIT exit from MVBs. On the other hand, the EGF-induced transport of EGFR, another RTK, to the lysosome was not affected in *Smap1*$^{-/-}$ MEFs (Figure 5D). Therefore, an ARF/SMAP1 system appears to be functioning in the MVB-to-lysosome transport of c-KIT but not that of EGFR.

*Smap1*$^{-/-}$ *aged mice develop phenotypes similar to those of myelodysplastic syndrome in humans.* The results described above (Figures 2–5) were based on MEFs from embryos and bone marrow cells from 2- to 4-month-old mice, and despite the alterations in membrane traffic, *Smap1*$^{-/-}$ mice were healthy up to the age of 12 months old. When Kaplan-Meier curves were plotted from the 35-month observation period, no statistically significant differences were detected between the survival percentages of *Smap1*-targeted and wild-type mice, although homozygously targeted mice showed a tendency to die at a somewhat younger age (Supplemental Figure 4A). Notably, a substantially higher percentage of homozygously targeted mice showed ill-health conditions after 12 months (Supplemental Figure 4B), suggesting the development of age-related diseases.

In fact, certain mice older than 1 year developed hematological disorders, and 33 of these *Smap1*$^{-/-}$ mice older than 1 year were analyzed by measuring the number of peripheral blood cells in each individual mouse (Table 1 and Supplemental Table 1). Based on the number of rbc, *Smap1*$^{-/-}$ mice were categorized into nonanemic and anemic/myelodysplastic syndrome (anemic/MDS) groups (100% and 70% rbc count as compared with wild type, respectively).

The average hematocrit and hemoglobin values in the anemic *Smap1*$^{-/-}$ group were lower (70%–75%) than those in the nonanemic *Smap1*$^{-/-}$ group and wild-type mice. MCV values were significantly increased in the anemic group, whereas MCH values did not differ significantly between the 2 groups, indicating the presence of macrocytic and normochromatic anemia in approximately half of *Smap1*$^{-/-}$ mice. A remarkable increase in the number of reticu-

**Table 2**
Summary of the hematological diagnosis seen in mice

| Genotype of mice | No. of mice | Age (mo.) | Diagnosis (no.) | Spleen weight (g) |
|---|---|---|---|---|
| *Smap1*$^{+/+}$ | 24 | 12–25 | Nonanemic (24) | 0.11 ± 0.07 |
| *Smap1*$^{-/-}$ | 33 | 13–25 | Nonanemic (16) | 0.10 ± 0.05 |
| | | | MDS (10) | 0.23 ± 0.16 |
| | | | MPD/MDS (2) | 0.68 ± 0.37 |
| | | | AML (5) | 0.99 ± 0.59 |

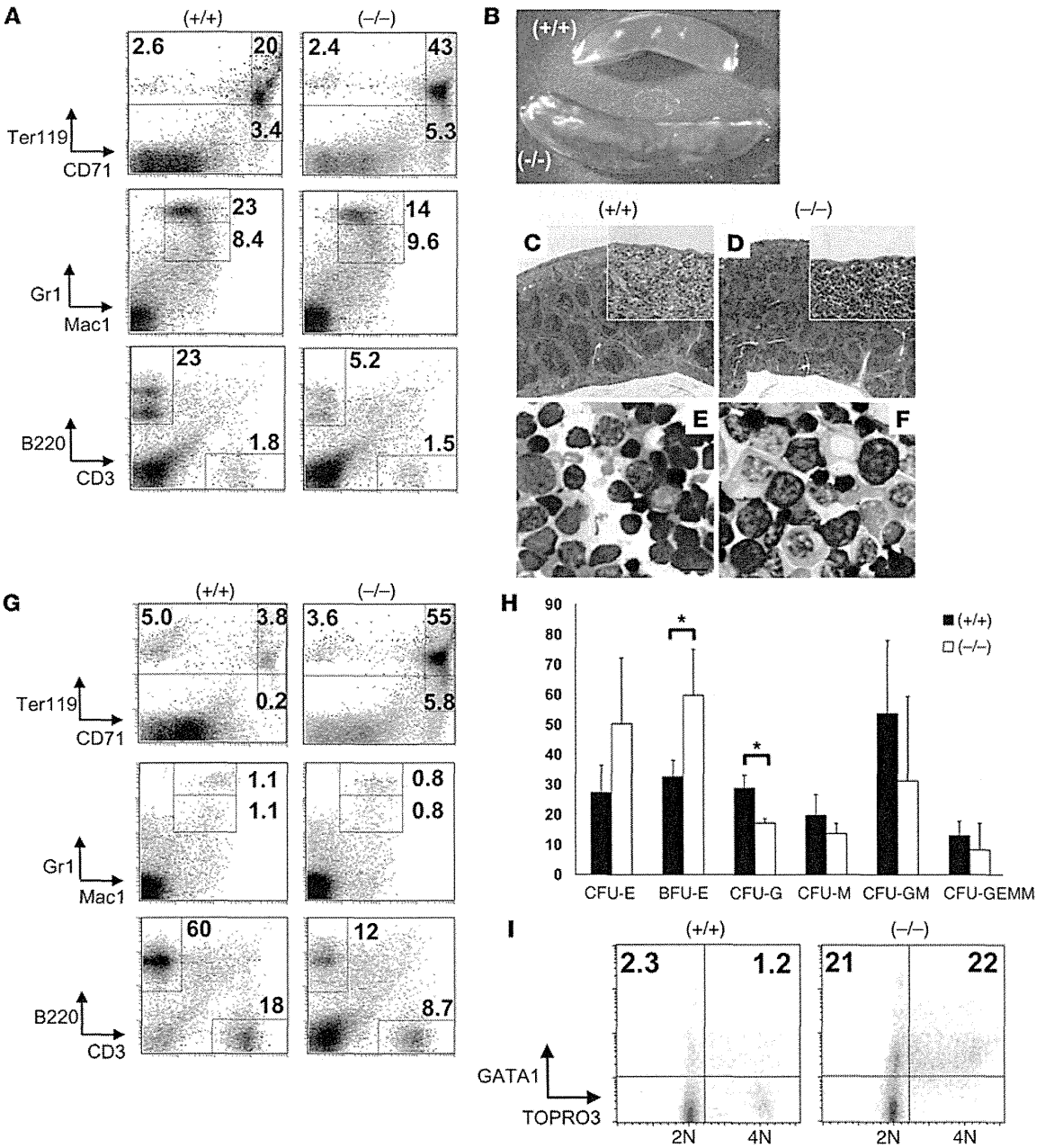


**Figure 7**

Enhanced erythropoiesis in *Smap1*$^{-/-}$ mice with MDS (ID no. 47; see Table 3). (**A** and **G**) Flow cytometry analyses of (**A**) bone marrow cells and (**G**) splenocytes prepared from *Smap1*$^{+/+}$ and *Smap1*$^{-/-}$ mice. The cells were stained for indicated hematopoietic lineage markers. The numbers represent percentages of cells in each gated box. Flow cytometry analyses were performed for all *Smap1*$^{-/-}$ mice with MDS, and reproducible results were obtained. (**B**–**F**) Histology of spleens. (**B**) A macroscopic view of the spleen. Note the enlargement of the *Smap1*$^{-/-}$ spleen. (**C** and **D**) Sections were stained by hematoxylin and eosin. Note the enrichment of cells with densely stained nuclei in the red pulp of the targeted spleen. (**E** and **F**) Smears of Giemsa-stained splenocytes. Erythroblasts with densely stained nuclei are evident in the *Smap1*$^{-/-}$ smear. Scale bar: 10 μm. (**H**) CFU-C assay of bone marrow cells. Cells from wild-type and *Smap1*$^{-/-}$ mice were assayed in vitro for their CFU-C activity. The numbers of colonies were counted under a microscope, and the morphology was classified as shown. Triplicate cultures were prepared from each mouse, and 4 independent pairs of older than 1 year *Smap1*$^{+/+}$ and *Smap1*$^{-/-}$ mice were used. The panel shows the averages ± SD of CFU-C values obtained from 12 cultures from each genotype. *$P < 0.0$. (**I**) Estimation of replicating cells in the spleen. Splenocytes from *Smap1*$^{+/+}$ and *Smap1*$^{-/-}$ mice were processed for flow cytometry analysis of GATA1 and TOPRO3. 2N and 4N represent the diploid and tetraploid status of chromatin.

**Table 3**
Details of the hematological disorder seen in *Smap1*$^{-/-}$ mice

| Mouse ID no. | Founder | Sex | Age (mo.) | Bone marrow | % Blasts in bone marrow cells[A] | Diagnosis |
|---|---|---|---|---|---|---|
| 47 | 44 | F | 13 | Erythroid hyperplasia | 2.9 | MDS |
| 675 | 64 | F | 15 | Erythroid hyperplasia | 0.4 | MDS |
| 834 | 44 | F | 18 | Erythroid hyperplasia | nd | MDS |
| 826 | 64 | F | 18 | Erythroid hyperplasia | 7.4 | MDS |
| 524 | 64 | F | 19 | Erythroid hyperplasia | 4.6 | MDS |
| 231 | 44 | F | 23 | Erythroid hyperplasia | 6.3 | MDS |
| 576 | 64 | M | 18 | Erythroid hyperplasia | 0.9 | MDS |
| 69 | 64 | F | 24 | ns | 3.4 | MDS |
| 72 | 64 | M | 17 | ns | nd | MDS |
| 199 | 64 | M | 25 | ns | 5.0 | MDS |
| 448 | 44 | F | 23 | Myeloproliferative | 12 | MPD/MDS |
| 518 | 64 | F | 17 | Myeloproliferative | 16 | MPD/MDS |
| 192 | 44 | F | 14 | Erythroleukemia | 28 | AML |
| 987 | 64 | F | 20 | Erythroleukemia | 24 | AML |
| 831 | 44 | F | 18 | Monocytic leukemia | 20 | AML |
| 34 | 64 | M | 19 | Monocytic leukemia | 22 | AML |
| 138 | 64 | F | 25 | Monocytic leukemia | 36 | AML |

[A]Note that the average percentage of blasts in bone marrow cells was 0.4 ± 0.3, as counted for 6 *Smap1*$^{+/+}$ mice. Numbers in the "Founder" column indicate the mouse line (the ES number). ns, no significant hyperplasia.

locytes was observed in the *Smap1*$^{-/-}$ anemic group, which likely reflects a mechanism of compensatory erythropoiesis. The number of platelets in *Smap1*$^{-/-}$ mice also decreased to 62%.

Peripheral blood and bone marrow cells from *Smap1*$^{-/-}$ mice were visualized using May-Grunwald-Giemsa staining (Figure 6), which revealed several morphological abnormalities mainly in erythrocytes and erythroid cells but also in megakaryocytic and even myeloid lineages (see the legend Figure 6 for details). Overall, the hematological disorders of *Smap1*$^{-/-}$ mice included (a) macrocytic and normochromatic anemia, (b) thrombocytopenia, and (c) abnormal cellular morphologies observed mainly in the erythroid lineage. These hematological disorders were detected exclusively in aged mice. Based on the Bethesda guidelines (20), these phenotypes correspond to features seen in MDS in aged humans.

Based on the above results, 10 *Smap1*$^{-/-}$ mice were diagnosed with MDS (Tables 1 and 2). Mice showing moribund conditions were sacrificed, and their bone marrow cells were examined by flow cytometry (Figure 7A). Erythroid lineage differentiation stages include Ter119$^{med}$CD71$^{hi}$ (proerythroblasts), Ter119$^{hi}$CD71$^{hi}$ (basophilic erythroblasts), and Ter119$^{hi}$CD71$^{med/lo}$ (late erythroblasts, including polychromatic/orthochromatic erythroblasts) (21). The Ter119$^{hi}$CD71$^{hi}$ fraction increased substantially in the *Smap1*$^{-/-}$ marrow as compared with the wild-type marrow (43% vs. 20%). In addition, the bone marrow from *Smap1*$^{-/-}$ mice showed hypercellularity, suggesting erythroid hyperplasia. Based on smears and flow cytometry, erythroid hyperplasia was detected in 7 out of 10 MDS-diagnosed *Smap1*$^{-/-}$ bone marrow samples (Table 3).

MDS-bearing *Smap1*$^{-/-}$ mice showed splenomegaly (Table 2), as illustrated in Figure 7B. Stained sections of *Smap1*$^{-/-}$ spleens (Figure 7D) revealed structurally intact red and white pulps, but the red pulp was extensively replaced by cells with densely stained nuclei. Splenocyte smears (Figure 7F) showed that the majority of these densely stained cells were erythroblasts. This was confirmed by flow cytometry analysis (Figure 7G), which revealed an increase in the Ter119$^{hi}$CD71$^{hi}$ fraction from 3.8% in the wild-type splenocytes to 55% in *Smap1*$^{-/-}$ splenocytes. Thus, splenomegaly seen in *Smap1*$^{-/-}$ mice most likely reflects erythroid hyperplasia.

To examine whether erythroid hyperplasia was accompanied by an enhancement of cell growth activity, a CFU assay was performed by in vitro culture of bone marrow cells (Figure 7H). BFU-E activity in *Smap1*$^{-/-}$ marrow cells was 1.8-fold higher than that in wild-type cells. This increase of BFU-E was apparent only in cells from mice older than 1 year of age, as shown in Figure 7H (data from younger mice is shown in Supplemental Figure 5). GATA1 is a master transcription factor of erythroid lineage. Splenocytes were stained for GATA1 expression and TOPRO3 (Figure 7I). In the *Smap1*-targeted spleen, the number of GATA1$^{+}$ cells with a DNA content above the diploid value (>2 N), which represent those undergoing DNA replication, increased to 22%.

The BFU-E assay and GATA1/TOPRO3 staining demonstrated that erythroid cell growth was enhanced in *Smap1*$^{-/-}$ mice. On the other hand, as shown above, these mice were characterized by anemia. Therefore, although erythropoiesis was enhanced in *Smap1*-targeted hematopoietic organs, the presence of morphological abnormalities in erythroid cells was indicative of a dysregulation of this process, resulting in overall ineffective erythropoiesis and eventually anemia.

*AML and myeloproliferative disease in Smap1-targeted mice.* In humans, patients with MDS often develop AML. We therefore assessed the incidence of AML in *Smap1*-targeted mice and found that 5 out of 33 *Smap1*$^{-/-}$ mice developed AML (Tables 1–3). Hematological subtypes of leukemia included erythroid (2 mice) and monocytic (3 mice). Figure 8A shows an example of a monocytic *Smap1*$^{-/-}$ AML mouse in which the liver and spleen were enlarged. Tissue sections of *Smap1*$^{-/-}$ mice (Figure 8B) show the infiltration of leukemic cells in the liver and spleen. Peripheral blood and bone marrow cell smears (Figure 8C) revealed the presence of immature monoblasts with large nuclei in the targeted mice. Figure 8, D and E, shows the results of flow cytometry analyses of bone marrow

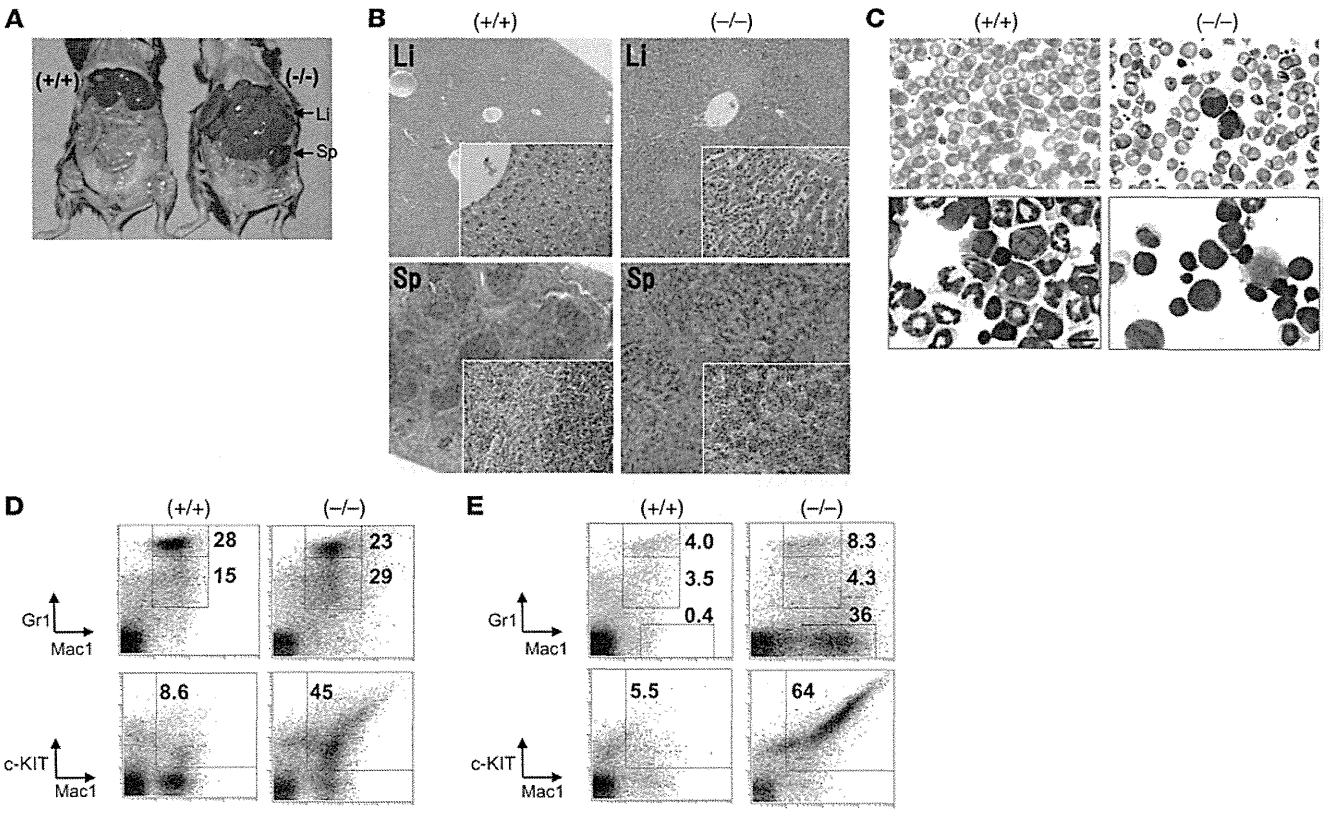


**Figure 8**

Monocytic AML in a *Smap1*$^{-/-}$ mouse (ID no. 831; see Table 3). (**A** and **B**) Macroscopic and histological views of the liver and spleen. Note the remarkably enlarged liver and spleen in the *Smap1*$^{-/-}$ mouse. Sections of liver and spleen were stained by hematoxylin and eosin. Note the massive infiltration of leukemic cells in the *Smap1*$^{-/-}$ tissues. The leukemic cells were relatively small in size and possessed densely stained nuclei. Original magnification, ×40; ×100 (insets). Li, liver; Sp, spleen. (**C**) Peripheral blood (top) and bone marrow cell (bottom) smears. Scale bar: 10 μm. (**D** and **E**) Flow cytometry analyses of (**D**) bone marrow cells and (**E**) splenocytes prepared from *Smap1*$^{+/+}$ and *Smap1*$^{-/-}$ mice. The cells were stained for hematopoietic lineage markers. The numbers indicate the percentage of cells in each gated box.

cells and splenocytes, respectively. *Smap1*$^{-/-}$ cells showed a substantial increase in the c-KIT$^{+}$Mac1$^{+}$ fraction (45% and 64% in bone marrow cells and splenocytes, respectively, as compared with 8.6% and 5.5% in the wild type) and an increase in the Gr1$^{-}$Mac1$^{+}$ fraction in the spleen (36% vs. 0.4% in the wild type). In addition, the immature Ter119$^{hi}$CD71$^{hi}$ fraction increased to 27% in the targeted spleen compared with 4.4% in the wild-type spleen (data not shown). This is likely the effect of enhanced compensatory erythropoiesis in response to anemia, suggesting the occurrence of AML in an MDS background. In fact, dysplastic cells were found in the peripheral blood smear (see *Smap1*$^{-/-}$ in Figure 8C).

In addition to monocytic leukemia, *Smap1*$^{-/-}$ mice developed erythroleukemia, as shown in Supplemental Figure 6. Overall, in the 5 mice that developed AML, the percentage of bone marrow blasts was above 20%, compared with 0.4%–7.4% in MDS-only mice (Table 2).

Two *Smap1*$^{-/-}$ mice developed a mixture of myeloproliferative disease (MPD) and MDS (Tables 1–3). The diagnosis of MPD was based on the increase in myeloid lineage cells, according to the Bethesda guidelines. Leukocytosis (as well as anemia and the presence of dysplastic cells) was observed in the peripheral blood, whereas in the bone marrow, the percentage of myeloid blasts was 12%–16%. Supplemental Figure 7 shows the results of analyses performed in a MPD *Smap1*$^{-/-}$ mouse.

*Role of c-KIT signaling in the growth of a Smap1*$^{-/-}$ *cell line derived from AML.* Finally, we examined the possible involvement of c-KIT signaling in the growth of *Smap1*$^{-/-}$ cells (Supplemental Figure 8). A cell line was established from the bone marrow of a monocytic AML mouse (ID no. 831; see Table 3). This cell line displayed a macrophage-like morphology and expressed c-KIT$^{lo}$, Mac1$^{hi}$, CD71$^{lo}$, and SCF (Supplemental Figure 8, A and B). Interestingly, as seen in Supplemental Figure 8C, which shows cells cultured without exogenous SCF, c-KIT was detected not only on the cell surface but also in the cytoplasm, and a fraction of cytoplasmic c-KIT colocalized with Hrs. In addition, treatment of cells with imatinib (a tyrosine kinase inhibitor) (22) or ISCK03 (a c-KIT inhibitor) (23) reduced cell viability and ERK1/2 phosphorylation (Supplemental Figure 8, D–F). Therefore, c-KIT signaling appears to have a positive effect on the viability of this AML-derived cell line.

## Discussion

We previously reported that the overexpression of SMAP1 impairs the endocytosis of the transferrin receptor in cultured cells (refs. 5, 6, and see Supplemental Figure 9 for the effects of SMAP1 overexpression on c-KIT transport). In this study, we confirmed that SMAP1 is similarly involved in transferrin endocytosis in mouse tissues but unexpectedly found that *SMAP1*-deleted cells (both erythroblasts

and MEFs) incorporated transferrin more efficiently than wild-type cells. One possible explanation for this enhanced endocytosis of transferrin is the upregulation of the active form of ARF6 in the absence of SMAP1. In this case, SMAP1 could be conferred a negative role in endocytosis. However, a number of reports provided evidence that, for vesicles to be formed properly, ARF has to exert its GTPase activity and itself be converted to an inactive form (24–28). Therefore, as an alternative mechanism of transferrin endocytosis, we hypothesized that endogenous SMAP1 could play a positive role by converting ARF6 to an inactive form and speculated the possible involvement of SMAP2, a SMAP1 homolog. Namely, SMAP1 deficiency might be accompanied by the mobilization of SMAP2 as a compensatory mechanism in *Smap1*-targeted cells (29). Since SMAP2 can function as an ARF1 GAP and exhibit higher GAP activity than SMAP1 (16), the recruitment of SMAP2 might lead to enhancement of transferrin endocytosis. This mechanism was supported by the abolishment of transferrin endocytosis in SMAP2-silenced *Smap1*$^{-/-}$ MEFs. A positive role for SMAP1 is compatible with the function of other ARF GAP proteins whose knockdown impairs vesicle transport. For example, targeting of ARF GAP1 impaired transferrin endocytosis (30), suggesting an ARF GAP1–dependent but SMAP1/2-independent route of transferrin endocytosis. In any case, our results support a positive role of SMAP1 in vesicle formation and may contribute to the discussion on the putative terminator versus effector functions of ARF GAPs (31, 32).

In this study, the loss of SMAP1 from BMMCs had no impact on SCF-mediated endocytosis of c-KIT, indicating that SMAP1 may play a role in the constitutive endocytosis of transferrin but not in the ligand-induced internalization of c-KIT. This result supports the idea that ARF GAP proteins function in distinctive, cargo-dependent pathways of endocytosis (33, 34). Alternatively, the present results may reveal a novel and possibly important function of SMAP1 in the degradation of c-KIT. SCF induces the phosphorylation and monoubiquitination of c-KIT, which are necessary for Grb2 association and endocytosis, respectively. The dephosphorylation of internalized RTKs occurs on early endosomes (7, 35). We observed that the kinetics of c-KIT in the early phases, such as phosphorylation, dephosphorylation, endocytosis from the cell surface, and exit from early endosomes, were not affected by the loss of SMAP1. In the late phases, c-KIT is transported to MVBs and eventually to the lysosomes (18, 19, 36). The endocytic adaptor protein Hrs functions at the MVB together with clathrin to sort ubiquitinated cargo to the lysosome (37, 38). Our results show that endogenous SMAP1 colocalized at least partially with clathrin and Hrs, suggesting that SMAP1 may be involved in the sorting of cargo at the MVB. In line with this notion, transport of c-KIT from MVB to lysosomes was substantially delayed in *Smap1*$^{-/-}$ cells. Importantly, undegraded c-KIT, ubiquitinated c-KIT, and Grb2-associated c-KIT increased in *Smap1*-targeted cells. Collectively, our results suggest that, in *Smap1*$^{-/-}$ cells, c-KIT persisting on MVBs may be in the dephosphorylated form but still capable of associating with Grb2, thereby leading to elevated levels of phosphorylated ERK. This suggests an enhancement of SCF-triggered c-KIT signaling, which was confirmed by an increase in thymidine uptake in these cells as an indicator of enhanced cell growth activity.

The alterations in transferrin and c-KIT transport discussed above were based on the analysis of *Smap1*-targeted cells derived from embryos and/or young mice exhibiting no obvious pathologies. We also revealed that aged *Smap1*-targeted mice exhibited phenotypes that resembled those of hematological disorders in human patients with MDS. Importantly, the signs of MDS were observed in 50% of *Smap1*-targeted aged mice, suggesting that disturbances in membrane transport may act as a predisposing but not a deterministic factor for MDS development. For MDS to occur, a genetic alteration may need to be present in addition to *SMAP1* deficiency.

The MDS-like features observed in *Smap1*-targeted mice included anemia, thrombocytopenia, and the presence of dysplastic blood cells. The majority of these mice showed signs of accelerated erythropoiesis in the bone marrow and spleen, which were confirmed by an increase in the number of erythroid-committed progenitors. Erythroid cells may have acquired enhanced proliferation abilities associated with differentiation defects, resulting in the occurrence of anemia. Enhanced expression of *SMAP1* in the MEPs and Ter119$^{+}$ fractions is in good accordance with the erythroid lineage-specific effects of *SMAP1* targeting.

Patients with MDS are particularly prone to developing AML. In this study, *Smap1*-targeted mice developed a range of AML subtypes, such as erythroid and monocytic leukemia. This is consistent with the notion that, in humans, MDS clones arise in CD34$^{+}$ progenitor cells (39) and with the observation that *SMAP1* expression is detected broadly in various hematopoietic lineages. Several *Smap1*$^{-/-}$ animals that had been diagnosed with MDS in our study subsequently developed AML (data not shown). It must be noted that not all MDS mice progressed to AML. This suggests that an additional genetic alteration(s) might be necessary to fully confer AML phenotypes. Screening and identification of such secondary mutations might provide information on the possible cooperation between *SMAP1* and another gene, resulting in the progression from MDS to AML.

Several clathrin-related molecules have been reported to enhance both transferrin endocytosis and cell growth. Huntingtin-interacting protein 1 (HIP1) is a clathrin-associated protein, and its expression level is frequently elevated in primary human cancers. In addition, overexpression of HIP1 alters the distribution patterns of clathrin and the AP-2 adaptor protein and promotes endocytosis of the transferrin receptor (40). Hrb/AGFG, another ARF GAP, functions positively in transferrin endocytosis in leukemic cells overexpressing Notch (41). It is widely accepted that transferrin receptor expression is increased in malignant tumors, including hematological malignancies, and may promote cell growth (42–44). Therefore, the enhanced endocytosis of transferrin in *Smap1*-targeted mice might facilitate the active iron metabolism and c-KIT–induced growth of erythroblasts and MDS/AML cells.

Furthermore, certain molecules that regulate the endocytosis of RTKs, such as c-KIT, have been associated with several human cancers. *c-Cbl* encodes an E3 ligase that ubiquitinates RTKs and is mutated in some cases of human MDS/AML (45, 46). Tsg101 is a component of the ESCRT-1 complex that functions downstream of Hrs to sort ubiquitinated RTKs to MVBs. In various human cancers, *TSG101* is deleted or its splicing pattern is altered (7, 47). Furthermore, *SMAP1* is frequently mutated in human colon cancer associated with microsatellite instability (15). Base deletion or addition in the $(A)_{10}$ repeat causes a frameshift in the ARF GAP domain, resulting in a loss-of-function type mutation of *SMAP1* (occurrence of colon cancer has not been observed in our *Smap1*$^{-/-}$ mice so far). Although one case of a *MLL-SMAP1* chimeric gene was reported in monocytic AML, the possible involvement of *SMAP1* in human MDS/AML remains to be investigated in the future.

In summary, this study revealed the predisposing role of alterations in clathrin-dependent protein trafficking in the development of MDS (and subsequent AML). To the best of our knowledge, this is the first report describing this mechanism using a mouse model.

## Methods

*Mice.* The 4.8-kb and 6.4-kb fragments corresponding to the 5′ and 3′ sequences, respectively, of exon 1 of *SMAP1* were obtained from the corresponding BAC clones by appropriate restriction digestion. The genomic fragments, as well as the loxP site, *frt*-flanked neomycin resistance cassette, and diphtheria toxin subunit A gene, were inserted into the targeting vector. The resulting plasmid DNA was linearized and electrophoretically transfected into TT2 ES cells, which were derived from an F1 mouse of a C57BL/6 and CBA mating (48). Positive and negative selection and PCR genotyping yielded 14 colonies. Recombinant alleles were detected by PCR screening using the forward and reverse primers (5′-CTGACCGCTTCCTCGTGCTTTACG-3′ and 5′-AATACACATGGCCTAGATATTAACCTATAG-3′) derived from the neomycin resistance cassette and 3′ external region. Recombination was verified by Southern blot analysis, and 3 independent clones were each injected into 8-cell stage embryos of CD-1 mice. Two clones, 44 and 64, were successfully transmitted through the germ line, and *Smap1*-heterozygous mice were backcrossed to C57BL/6 mice for more than 10 generations. During these matings, heterozygous mice were crossed with *E2A-Cre* transgenic mice, causing the deletion of exon 1 in all tissues. *Smap1*$^{+/-}$ mice (acc. no. CDB0427K; http://www.cdb.riken.jp/arg/mutant%20mice%20list.html) were thus established. For PCR genotyping of mice, the reverse primer was 5′-CCTCTGCTAACTCTACTCAG-3′, and the forward primers were 5′-GTCATCCTGGTTAGCCTCAGTCTTG-3′ for the wild-type alleles, 5′-CGCCTTCTATCGCCTTCTTGACG-3′ for the floxed alleles, and 5′-CCTGCCCTTACCCAGACTGTCTTAG-3′ for the targeted alleles. The expected sizes of PCR products were 330 bp, 554 bp, and 480 bp for wild-type, floxed, and targeted alleles, respectively. Mice were maintained in the Animal Facility of the Institute of Development, Aging, and Cancer, Tohoku University, an environmentally controlled and specific pathogen-free facility.

*Cultures of BMMCs, the AML-derived cell line, and MEFs.* Femoral bone marrow cells were cultured in RPMI1640 supplemented with 10% (v/v) FBS, 2 mM L-glutamine, 50 μM 2-mercaptoethanol, 10 mM HEPES (pH 7.4), 0.2 mM nonessential amino acids, 1 mM sodium pyruvate, 100 U/ml penicillin, and 100 μg/ml streptomycin. The cytokines added were 20 ng/ml IL-3 and 10 ng/ml SCF for the first 2 weeks followed by 20 ng/ml IL-3 only for the next 2 weeks. The purity of BMMCs reached over 95%, as assessed by the surface expression of c-KIT and FcεRI. A cell line was established from the bone marrow of an AML-bearing *Smap1*$^{-/-}$ mouse (ID no. 831; see Table 3) and cultured (deposited as TKG 0661 at the Cell Resource Center for Biomedical Research, Institute of Development, Aging and Cancer, Tohoku University). The medium was the same as that used for BMMCs but without any cytokine added. Cell viability was measured using a Cell Counting Kit-8 (Dojindo). In the indicated cases, cells were treated with imatinib mesylate (Santa Cruz Biotechnology Inc.) or ISCK03 (Sigma-Aldrich).

MEFs were prepared according to a previously published procedure (49). Briefly, 16.5-day-old embryos were isolated from pregnant mice. Single cell suspensions were prepared by trypsin digestion, cultured in a monolayer in DMEM supplemented with serum for 3 days, and immortalized by transfection with the SV40 large T antigen. Two independent cultures were established for wild-type and *Smap1*$^{-/-}$ genotypes. Two siRNAs against SMAP2, siRNA1 and siRNA2, were purchased from Japan BioServices Co. LTD. and used to downregulate endogenous SMAP2 in MEFs. The sequences of siRNA1 and siRNA2 were 5′-GGAUUUAUUCGAGAUAAAUTT-3′ and 5′-CCUGUUGUUUUUGAGAAAGTT-3′, respectively.

*Hematological and histological examination.* Peripheral blood was collected from the tail veins of mice, and hematological parameters were measured using an automated cell counter (XT-4000i, Sysmex). Smears of peripheral blood and bone marrow cells were prepared on glass slides and stained with May-Grunwald-Giemsa (Wako). Tissues, such as those derived from the spleen and liver, were fixed in 4% (w/v) paraformaldehyde in PBS for 18 hours at 4°C and embedded in paraffin. Microsections of each specimen were fixed on glass slides, deparaffinized, and stained with hematoxylin and eosin (Wako).

*Flow cytometry analyses.* Single cell suspensions were prepared from the bone marrow and spleen and incubated with CD16/32 mAb (BD Pharmingen) for 15 minutes, followed by incubation with an appropriately diluted, fluorescein-conjugated mAb on ice for 30 minutes. The mAbs used were PE-anti-CD71 (eBioscience) and FITC-anti-c-KIT, PE-anti-Ter119, APC-anti-Ter119, PE-anti-Gr1, APC-anti-Mac1, APC-anti-B220, and FITC-anti-CD3ε (all from BD Pharmingen). For DNA labeling, cells were fixed in 4% (w/v) paraformaldehyde in PBS and permeabilized with 0.25% (v/v) Triton X-100 and 5% (w/v) DMSO in PBS. After blocking with 10% (v/v) goat serum in PBS, cells were incubated with anti-GATA1 mAb (Santa Cruz Biotechnology Inc.) and TOPRO3 (Molecular Probes), followed by a secondary antibody reaction. The labeled cells were separated with an analytical flow cytometer (Beckman Coulter), and the data were analyzed with EXPO32 software. Various hematopoietic progenitor fractions were identified using the appropriate antibodies. These populations were designated as follows: KSL, Lin$^-$/c-KIT$^+$/Sca-1$^+$; FLT3-KSL, Lin$^-$/c-KIT$^+$/Sca-1$^+$/FLT3$^-$; FLT3+KSL, Lin$^-$/c-KIT$^+$/Sca-1$^+$/FLT3$^+$; CMP, Lin$^-$/c-KIT$^+$/Sca-1$^-$/CD34$^{hi}$/FcγR$^{lo}$; GMP, Lin$^-$/c-KIT$^+$/Sca-1$^-$/CD34$^{hi}$/FcγR$^{hi}$; and MEP, Lin$^-$/c-KIT$^+$/Sca-1$^-$/CD34$^{lo}$/FcγR$^{lo}$. Cell sorting was performed using a FACSAria (Becton Dickinson).

*Colony formation and $^3$H-thymidine incorporation assays.* Single cell suspensions were prepared from the femoral bone marrow and plated at a density of 1 × 10$^4$ cells per ml of methylcellulose (M3234, Stem Cell Technologies) in a 3.5-cm-diameter dish. The culture medium contained 50 ng/ml rmSCF (Kirin Brewery Company Ltd.), 10 ng/ml rmIL-3 (Wako), 10 ng/ml rmIL-6 (Wako), and 3 U/ml rhEPO (Peprotech). Colonies formed were observed through a phase-contrast microscope, and their numbers were counted on the third day for CFU-E and twelfth day for BFU-E, CFU-G, CFU-M, CFU-GM, and CFU-GEMM. In certain cases, 20 kBq of $^3$H-thymidine (GE Healthcare) was added to the culture of 2 × 10$^4$ BMMCs for 8 hours, and its incorporation into an acid-insoluble fraction was measured by a beta-counter, Matrix 9600 (Packard), according to the described method (50).

*Transport assay.* Intracellular uptake and recycling of transferrin were evaluated using an erythroblast-containing fraction. Bone marrow cells were incubated in serum-free medium at 37°C for 2 hours and then in RPMI1640 containing 50 μg/ml Alexa Fluor 488–conjugated transferrin (Molecular Probes), 20 mM HEPES (pH 7.4), and 1% (w/v) BSA on ice for 30 minutes. After washing 3 times, transferrin internalization was induced by incubating cells in RPMI1640 containing 10% (v/v) FBS at 37°C for the indicated times. Transferrin remaining on the plasma membrane was removed by incubating cells in a prechilled buffer consisting of 20 mM MES (pH 5), 130 mM NaCl, 50 μM deferoxamine, 2 mM $CaCl_2$, and 0.1% (w/v) BSA on ice for 20 minutes. After washing 3 times, cells were labeled with PE-anti-Ter119, and the fluorescence intensity of internalized transferrin in each Ter119$^+$ fraction was quantified by flow cytometry.

For measuring the internalization of c-KIT, BMMCs were first serum starved and then incubated in RPMI1640 supplemented with 100 ng/ml SCF and 0.1% (w/v) BSA in the presence of 100 μg/ml cycloheximide (Sigma-Aldrich), and the c-KIT remaining on the cell surface was measured by flow cytometry.

Transferrin internalization in MEFs was measured by adjusting the procedure to a monolayer culture. MEFs were incubated in serum-free medium at 37°C for 2 hours and then in the presence of dye-conjugated transferrin at 37°C for various time periods. After treatment of cells with an acid buffer to remove cell surface transferrin, cells were harvested by trypsin-EDTA treatment and processed for flow cytometry. In the indicated cases, endocytosis and recycling were measured separately using biotinylated transferrin that was prepared by coupling Holo-Transferrin (R&D Systems) and NHS-SS-biotin (Thermo SCIENTIFIC). In the internalization assay, MEFs grown on gelatin-coated dishes were incubated in serum-free medium at 37°C for 2 hours and then in the presence of 20 μg/ml biotinylated transferrin for 30 minutes at 4°C, washed, and further incubated at 37°C for various times. Then, the surface-bound biotinylated transferrin was stripped by treating cells with 50 mM sodium 2-mercaptoethane sulfonate (MESNA) in TNB buffer (50 mM Tris-HCl [pH 8.6], 100 mM NaCl, 0.2% [w/v] BSA) for 30 minutes at 4°C, and MESNA was quenched by 75 mM iodoacetamide in TNB buffer for 30 minutes at 4°C. Lysates were prepared in lysis buffer (10 mM Tris-HCl [pH 7.4], 50 mM NaCl, 1 mM EDTA, 0.2% [w/v] BSA, 0.1% [w/v] SDS, 1% [v/v] Triton X-100) and applied to ELISA plates coated with anti-transferrin antibodies. After washing, antibody-trapped biotinylated transferrin was detected using HRP-conjugated streptavidin (DAKO). In the recycling assay, MEFs were incubated with 20 μg/ml biotinylated transferrin for 40 minutes at 37°C, followed by reduction with MESNA and incubation with 200 μg/ml unlabeled transferrin at 37°C for various times. Preparation of cell lysates and ELISA were the same as that above.

To monitor endocytosis and intracellular transport of c-KIT, MEFs were transfected by signal sequence-tagged EYFP-c-KIT (51) (provided by J. Duyster, Technical University of Munich, Munich, Germany) using a 4D-Nucleofector System (Lonza), incubated with 100 ng/ml SCF for different times, fixed with 4% (w/v) paraformaldehyde in PBS, permeabilized with 0.1 (v/v) Triton X-100 in PBS, and then processed for immunofluorescence detection. To examine the possible involvement of ARF GTPases in the intracellular transport of internalized c-KIT, COS7 cells were transfected with dominant-active forms of ARF1(Q71A), ARF5(Q71A), or ARF6(Q67A) (provided by K. Nakayama, Kyoto University, Kyoto, Japan) together with EYFP-c-KIT. To monitor the internalization of the EGFR, MEFs were incubated with 100 μg/ml Alexa Fluor 488–conjugated EGF (Molecular Probes).

*Immunoblotting, immunofluorescence, and RT-PCR.* The immunoblotting and immunofluorescence protocols used were as previously described (6). Anti-SMAP1 and anti-SMAP2 antibodies were purchased from Sigma-Aldrich. Anti-SMAP1 antibody was raised against amino acids 210–306 of the SMAP1 protein (440 amino acids), as specified by the manufacturer. The mAbs used were as follows: anti-panARF (Affinity Bioreagents); anti-clathrin heavy chain (Thermo Fisher Scientific); anti-c-KIT and anti-ARF6 (both from Santa Cruz Biotechnology Inc.); anti-ubiquitinated proteins (BIOMOL); anti-Rab11, anti-EEA1, anti-Grb2, and anti–phospho-tyrosine (all from BD Transduction Labs); anti-Rab5, anti-Rab7, anti-phosphorylated ERK1/2, and anti-ERK1/2 (all from Cell Signaling Technology); anti-Hrs (provided by N. Tanaka, Miyagi Cancer Research Center, Natori, Japan); and anti-LBPA (provided by T. Kobayashi, Riken Institute, Wako, Japan). Lysotracker was purchased from Molecular Probes. For immunoprecipitation, BMMCs were lysed with a buffer consisting of 25 mM HEPES-KOH (pH 7.4), 150 mM NaCl, 5 mM EDTA, 1% (v/v) Triton X-100, 2 mM DTT, 5 mM NaF, 5 mM $Na_2VO_4$, and a mixture of protease inhibitors (Roche Diagnostics). The cellular fluorescence intensities and extent of fluorescence colocalization were measured using a confocal microscope, LSM-510, and the LSM5 Image Examiner tool (Zeiss). Colocalization coefficient was calculated as the ratio of $pixels^{colocalized\ c\text{-}Kit}$/$pixels^{total\ c\text{-}Kit}$. For RT-PCR, RNA was extracted from isolated cells using the TRIzol reagent and reverse transcribed using SSRT II (Invitrogen). The primers used were as follows: for *SMAP1*, 5′-CTGAGGGAGGAGGACAACAAGTAC-3′ (forward on exon 1), 5′-GAAGCCAATCTTCCAGAGAAC-3′ (forward on exon 3), and 5′-GTAACGGTAGACAGGGTAGCAGGT-3′ (reverse on exon 9); for *SCF*, 5′-GAAGAAAACGCACCGAAGAA-3′ (forward) and 5′-TAAGGCTCCAAAAGCAAAGC-3′ (reverse).

*Pull-down assay using GST-GGA1.* A *DH5α* strain of *E. coli* was transformed by a *GST-GGA1* fusion cDNA (52) (provided by K. Nakayama). Bacteria were grown in LB media and treated with 0.4 mM IPTG for 60 minutes to induce protein expression. Cells were lysed in B-PER buffer (Pierce), and the lysate was centrifuged to obtain a supernatant containing GST-GGA1. Bone marrow cells were lysed with a buffer consisting of 150 mM KCl, 2 mM $MgCl_2$, 10% (v/v) glycerol, 1 mM DTT, 1 mM EGTA, 1 mM EDTA, 1% (v/v) Triton X-100, 50 mM Tris-HCl (pH 8.0), and 1× protease inhibitors and incubated with purified GST-GGA1 that had been coupled with glutathione-Sepharose beads (Pierce). The bound protein was recovered by eluting with SDS-loading buffer and processed for immunoblot analyses.

*Statistics.* Statistical significance was evaluated using 2-tailed Student's *t* test, and differences of $P < 0.05$ were considered statistically significant.

*Study approval.* Animal protocols were reviewed and approved by the Animal Studies Committee of the Tohoku University.

## Acknowledgments

This work was supported by research grants from the Ministry of Education, Science, Sports, Culture and Technology of Japan; Gonryo Medical Foundation; and the Creative Interdisciplinary Research Program of the Center for Interdisciplinary Research, Tohoku University, Japan. M. Satake is supported by a GCOE program, "Network Medicine," at Tohoku University.

Received for publication March 5, 2012, and accepted in revised form January 3, 2013.

Address correspondence to: Masanobu Satake, Department of Molecular Immunology, Institute of Development, Aging and Cancer, Tohoku University, Seiryo-machi 4-1, Aoba-ku, Sendai 980-8575, Japan. Phone: 81.22.717.8477; Fax: 81.22.717.8482; E-mail: satake@idac.tohoku.ac.jp.

1. D'Souza-Schorey C, Chavrier P. ARF proteins: roles in membrane traffic and beyond. *Nat Rev Mol Cell Biol.* 2006;7(5):347–358.
2. Donaldson JG, Jackson CL. ARF family G proteins and their regulators: roles in membrane transport, development and disease. *Nat Rev Mol Cell Biol.* 2011;12(6):362–375.
3. Donaldson JG. Multiple roles for Arf6: sorting, structuring, and signaling at the plasma membrane. *J Biol Chem.* 2003;278(43):41573–41576.
4. Gillingham AK, Munro S. The small G proteins of the Arf family and their regulators. *Annu Rev Cell Dev Biol.* 2007;23:579–611.
5. Tanabe K, Torii T, Natsume W, Braesch-Andersen S, Watanabe T, Satake M. A novel GTPase-activating protein for ARF6 directly interacts with clathrin and regulates clathrin-dependent endocytosis. *Mol Biol Cell.* 2005;16(4):1617–1628.
6. Kon S, Tanabe K, Watanabe T, Sabe H, Satake M. Clathrin dependent endocytosis of E-cadherin is regulated by the Arf6GAP isoform SMAP1. *Exp Cell Res.* 2008;314(7):1415–1428.
7. Bache KG, Slagsvold T, Stenmark H. Defective downregulation of receptor tyrosine kinases in cancer. *EMBO J.* 2004;23(14):2707–2712.
8. Crosetto N, Tikkanen R, Dikic I. Oncogenic breakdowns in endocytic adaptor proteins. *FEBS Lett.* 2005;579(15):3231–3238.
9. Lanzetti L, Di Fiore PP. Endocytosis and cancer: an 'insider' network with dangerous liaisons. *Traffic.* 2008;9(12):2011–2021.
10. McMahon HT, Boucrot E. Molecular mechanism and physiological functions of clathrin-mediated endocytosis. *Nat Rev Mol Cell Biol.* 2011;12(8):517–533.
11. Kalesnikoff J, et al. RabGEF1 regulates stem cell factor/c-Kit-mediated signaling events and biological responses in mast cells. *Proc Natl Acad Sci U S A.* 2006;103(8):2659–2664.
12. Sigismund S, Argenzio E, Tosoni D, Cavallaro E, Polo

S, Di Fiore PP. Clathrin-mediated internalization is essential for sustained EGFR signaling but dispensable for degradation. *Dev Cell.* 2008;15(2):209–219.
13. Joffre C, Barrow R, Ménard L, Calleja V, Hart IR, Kermorgant S. A direct role for Met endocytosis in tumorigenesis. *Nat Cell Biol.* 2011;13(7):827–837.
14. Meyer C, et al. Diagnostic tool for the identification of MLL rearrangements including unknown partner genes. *Proc Natl Acad Sci U S A.* 2005;102(2):449–454.
15. El-Bchiri J, et al. Nonsense-mediated mRNA decay impacts MSI-driven carcinogenesis and anti-tumor immunity in colorectal cancers. *PLoS One.* 2008;3(7):e2583.
16. Natsume W, et al. SMAP2, a novel ARF GTPase-activating protein, interacts with clathrin and clathrin assembly protein and functions on the AP-1-positive early endosome/trans-Golgi network. *Mol Biol Cell.* 2006;17(6):2592–2603.
17. Collins BM, Watson PJ, Owen DJ. The structure of the GGA1-GAT domain reveals the molecular basis for ARF binding and membrane association of GGAs. *Dev Cell.* 2003;4(3):321–332.
18. Sorkin A, Von Zastrow M. Signal transduction and endocytosis: close encounters of many kinds. *Nat Rev Mol Cell Biol.* 2002;3(8):600–614.
19. Masson K, Heiss E, Band H, Ronnstrand L. Direct binding of Cbl to Tyr568 and Tyr936 of the stem cell factor receptor/c-Kit is required for ligand-induced ubiquitination, internalization and degradation. *Biochem J.* 2006;399(1):59–67.
20. Kogan SC. Bethesda proposals for classification of nonlymphoid hematopoietic neoplasms in mice. *Blood.* 2002;100(1):238–245.
21. Socolovsky M. Ineffective erythropoiesis in Stat5a$^{-/-}$ 5b$^{-/-}$ mice due to decreased survival of early erythroblasts. *Blood.* 2001;98(12):3261–3273.
22. Heinrich MC, Griffith DJ, Druker BJ, Wait CL, Ott KA, Zigler AJ. Inhibition of c-kit receptor tyrosine kinase activity by STI 571, a selective tyrosine kinase inhibitor. *Blood.* 2000;96(3):925–932.
23. Na YJ, Baek HS, Ahn SM, Shin HJ, Chang IS, Hwang JS. [4-t-butylphenyl]-N-(4-imidazol-1-yl phenyl)sulfonamide (ISCK03) inhibits SCF/c-kit signaling in 501mel human melanoma cells and abolishes melanin production in mice and brownish guinea pigs. *Biochem Pharmacol.* 2007;74(5):780–786.
24. Lanoix J, et al. Sorting of Golgi resident proteins into different subpopulations of COPI vesicles: a role for ArfGAP1. *J Cell Biol.* 2001;155(7):1199–1212.
25. Yang JS, et al. ARFGAP1 promotes the formation of COPI vesicles, suggesting function as a component of the coat. *J Cell Biol.* 2002;159(1):69–78.
26. Lee SY, Yang JS, Hong W, Premont RT, Hsu VW. ARFGAP1 plays a central role in coupling COPI cargo sorting with vesicle formation. *J Cell Biol.* 2005;168(2):281–290.
27. Kahn RA. Toward a model for Arf GTPases as regulators of traffic at the Golgi. *FEBS Lett.* 2009;583(23):3872–3879.
28. Spang A, Shiba Y, Randazzo PA. Arf GAPs: gatekeepers of vesicle generation. *FEBS Lett.* 2010;584(12):2646–2651.
29. Sakakura I, Tanabe K, Nouki N, Suzuki M, Satake M, Watanabe T. The carboxy-terminal region of SMAP2 directs subcellular localization as well as Arf protein specificity. *Biochem Biophys Res Commun.* 2011;404(2):661–666.
30. Bai M, et al. ARFGAP1 promotes AP-2-dependent endocytosis. *Nat Cell Biol.* 2011;13(5):559–567.
31. Kahn RA. GAPs: Terminator versus effector functions and the role(s) of ArfGAP1 in vesicle biogenesis. *Cell Logist.* 2011;1(2):49–51.
32. Kon S, Funaki T, Satake M. Putative terminator and/or effector functions of Arf GAPs in the trafficking of clathrin-coated vesicles. *Cell Logist.* 2011;1(3):86–89.
33. Randazzo PA, Hirsch DS. Arf GAPs: multifunctional proteins that regulate membrane traffic and actin remodelling. *Cell Sig.* 2004;16(4):401–413.
34. Tanabe K, Kon S, Natsume W, Torii T, Watanabe T, Satake M. Involvement of a novel ADP-ribosylation factor GTPase-activating protein, SMAP, in membrane trafficking: implications in cancer cell biology. *Cancer Sci.* 2006;97(9):801–806.
35. Authier F, Chauvet G. In vitro endosome-lysosome transfer of dephosphorylated EGF receptor and Shc in rat liver. *FEBS Lett.* 1999;461(1–2):25–31.
36. Zeng S, Xu Z, Lipkowitz S, Longley JB. Regulation of stem cell factor receptor signaling by Cbl family proteins (Cbl-b/c-Cbl). *Blood.* 2005;105(1):226–232.
37. Raiborg C, Bache KG, Mehlum A, Stang E, Stenmark H. Hrs recruits clathrin to early endosomes. *EMBO J.* 2001;20(17):5008–5021.
38. Raiborg C, Bache KG, Gillooly DJ, Madshus IH, Stang E, Stenmark H. Hrs sorts ubiquitinated proteins into clathrin-coated microdomains of early endosomes. *Nat Cell Biol.* 2002;4(5):394–398.
39. Corey SJ, Minden MD, Barber DL, Kantarjian H, Wang JC, Schimmer AD. Myelodysplastic syndromes: the complexity of stem-cell diseases. *Nat Rev Cancer.* 2007;7(2):118–129.
40. Rao DS, et al. Altered receptor trafficking in Huntingtin interacting protein 1-transformed cells. *Cancer Cell.* 2003;3(5):471–482.
41. Khwaja SS, et al. HIV-1 Rev-binding protein accelerates cellular uptake of iron to drive Notch-induced T cell leukemogenesis in mice. *J Clin Invest.* 2010;120(7):2537–2548.
42. Smilevska T, et al. Transferrin receptor-1 and 2 expression in chronic lymphocytic leukemia. *Leuk Res.* 2006;30(2):183–189.
43. O'Donnell KA, et al. Activation of transferrin receptor 1 by c-Myc enhances cellular proliferation and tumorigenesis. *Mol Cell Biol.* 2006;26(6):2373–2386.
44. Habashy HO, et al. Transferrin receptor (CD71) is a marker of poor prognosis in breast cancer and can predict response to tamoxifen. *Breast Cancer Res Treat.* 2010;119(2):283–293.
45. Caligiuri MA, et al. Novel c-CBL and CBL-b ubiquitin ligase mutations in human acute myeloid leukemia. *Blood.* 2007;110(3):1022–1024.
46. Sanada M, et al. Gain-of-function of mutated C-CBL tumour suppressor in myeloid neoplasms. *Nature.* 2009;460(7257):904–908.
47. Tanaka N, Kyuuma M, Sugamura K. Endosomal sorting complex required for transport proteins in cancer pathogenesis, vesicular transport, and non-endosomal functions. *Cancer Sci.* 2008;99(7):1293–1303.
48. Yagi T, et al. A novel ES cell line, TT2, with high germline-differentiating potency. *Anal Biochem.* 1993;214(1):70–76.
49. Funaki T, et al. Localization of SMAP2 to the TGN and its function in the regulation of TGN protein transport. *Cell Struct Funct.* 2011;36(1):83–95.
50. Endo S, Sakamoto Y, Kobayashi E, Nakamura A, Takai T. Regulation of cytotoxic T lymphocyte triggering by PIR-B on dendritic cells. *Proc Natl Acad Sci U S A.* 2008;105(38):14515–14520.
51. Jahn T, et al. Analysing c-kit internalization using a functional c-kit-EGFP chimera containing the fluorochrome within the extracellular domain. *Oncogene.* 2002;21(29):4508–4520.
52. Takatsu H, Yoshino K, Toda K, Nakayama K. GGA proteins associate with Golgi membranes through interaction between their GGAH domains and ADP-ribosylation factors. *Biochem J.* 2002; 365(pt 2):369–378.

# *ACTN1* Mutations Cause Congenital Macrothrombocytopenia

Shinji Kunishima,[1,*] Yusuke Okuno,[2,3] Kenichi Yoshida,[2] Yuichi Shiraishi,[4] Masashi Sanada,[2] Hideki Muramatsu,[3] Kenichi Chiba,[4] Hiroko Tanaka,[4] Koji Miyazaki,[5] Michio Sakai,[6] Masatoshi Ohtake,[7] Ryoji Kobayashi,[8] Akihiro Iguchi,[9] Gen Niimi,[10] Makoto Otsu,[11] Yoshiyuki Takahashi,[3] Satoru Miyano,[4] Hidehiko Saito,[12] Seiji Kojima,[3] and Seishi Ogawa[2]

Congenital macrothrombocytopenia (CMTP) is a heterogeneous group of rare platelet disorders characterized by a congenital reduction of platelet counts and abnormally large platelets, for which CMTP-causing mutations are only found in approximately half the cases. We herein performed whole-exome sequencing and targeted Sanger sequencing to identify mutations that cause CMTP, in which a dominant mode of transmission had been suspected but for which no known responsible mutations have been documented. In 13 Japanese CMTP-affected pedigrees, we identified six (46%) affected by *ACTN1* variants cosegregating with CMTP. In the entire cohort, *ACNT1* variants accounted for 5.5% of the dominant forms of CMTP cases and represented the fourth most common cause in Japanese individuals. Individuals with *ACTN1* variants presented with moderate macrothrombocytopenia with anisocytosis but were either asymptomatic or had only a modest bleeding tendency. *ACTN1* encodes α-actinin-1, a member of the actin-crosslinking protein superfamily that participates in the organization of the cytoskeleton. In vitro transfection experiments in Chinese hamster ovary cells demonstrated that altered α-actinin-1 disrupted the normal actin-based cytoskeletal structure. Moreover, transduction of mouse fetal liver-derived megakaryocytes with disease-associated *ACTN1* variants caused a disorganized actin-based cytoskeleton in megakaryocytes, resulting in the production of abnormally large proplatelet tips, which were reduced in number. Our findings provide an insight into the pathogenesis of CMTP.

Congenital thrombocytopenia is a highly heterogeneous group of inherited disorders showing low platelet counts. A subgroup of these disorders is distinguished morphologically by the production of abnormally large platelets and is thus referred to as congenital macrothrombocytopenia (CMTP).[1–3] The clinical presentations of CMTP-affected individuals vary considerably and range from no symptoms to a severe bleeding tendency. Thus far, CMTP-causing mutations have been reported in more than 12 genes.[1–3] Among these, the most common is *MYH9* (MIM 160775), which is responsible for autosomal-dominant *MYH9* disorders or *MYH9*-related disease (MIM 153650, 153640, 600208, 155100, and 605249)[4,5] The second most common are *GP1BA* (MIM 606672), *GP1BB* (MIM 138720), and *GP9* (MIM 173515), which are responsible for autosomal-dominant (heterozygous) and -recessive (homozygous) Bernard-Soulier syndrome (MIM 231200).[6,7] Less frequent mutations have been reported in *FLI1* (MIM 193067),[8] *FLNA* (MIM 300017),[9] *GATA1* (MIM 305371),[10] *ITGA2B/ITGB3* (MIM 607759 and 173470),[11,12] *NBEAL2* (MIM 614169),[13–15] *TUBB1* (MIM 612901),[16] and *VWF* (MIM 613160).[17] However, even this array of mutations only accounts for approximately half the CMTP cases; in the remaining half, CMTP-causing mutations are unknown, which prevents a definite diagnosis of CMTP and potentially results in inappropriate treatments.[1–3]

To identify mutations that cause CMTP, we first performed whole-exome sequencing of genomic DNA from 11 affected and 10 unaffected individuals from six Japanese CMTP-affected families (Figure 1A) in which a dominant mode of transmission had been suspected but in which no relevant mutations in the previously reported genes had been identified (Figure S1, available online). The candidate mutations found in the exome sequencing were further examined for germline mutations in additional CMTP-affected pedigrees and/or individuals by high-throughput sequencing of PCR products from pooled DNA and subsequent validation by Sanger sequencing (Figure 1B). Written informed consent was obtained from all individuals in accordance with the Declaration of Helsinki. This study was approved by the institutional review boards of National Hospital Organization Nagoya Medical Center, The University of Tokyo, and Nagoya University.

For exome sequencing, genomic DNA from each member of the six pedigrees was enriched for protein-coding sequences with a SureSelect Human All Exon V3 kit (Agilent Technologies, Santa Clara, CA, USA). This was followed by massively parallel sequencing with the HiSeq 2000 platform with 100 bp paired-end reads

[1]Department of Advanced Diagnosis, Clinical Research Center, National Hospital Organization Nagoya Medical Center, Nagoya 4600001, Japan; [2]Cancer Genomics Project, Graduate School of Medicine, The University of Tokyo, Tokyo 1138655, Japan; [3]Department of Pediatrics, Nagoya University Graduate School of Medicine, Nagoya 4668550, Japan; [4]Laboratory of DNA Information Analysis, Human Genome Center, Institute of Medical Science, The University of Tokyo, Tokyo 1088639, Japan; [5]Department of Hematology, Kitasato University School of Medicine, Sagamihara, Kanagawa 2288555, Japan; [6]Department of Pediatrics, School of Medicine, University of Occupational and Environmental Health, Kitakyushu 8078555, Japan; [7]Division of Pediatrics, Sendai City Hospital, Miyagi 9848501, Japan; [8]Department of Pediatrics, Sapporo Hokuyu Hospital, Sapporo 0030006, Japan; [9]Department of Pediatrics, Hokkaido University Graduate School of Medicine, Sapporo 0608638, Japan; [10]Laboratory of Electron Microscopy, Joint Research Laboratory, Fujita Health University, Toyoake, Aichi 4701192, Japan; [11]Division of Stem Cell Therapy, Center for Stem Cell and Regenerative Medicine, Institute of Medical Science, The University of Tokyo, Tokyo 1088639, Japan; [12]National Hospital Organization Nagoya Medical Center, Nagoya 4600001, Japan
*Correspondence: kunishis@nnh.hosp.go.jp
http://dx.doi.org/10.1016/j.ajhg.2013.01.015. ©2013 by The American Society of Human Genetics. All rights reserved.

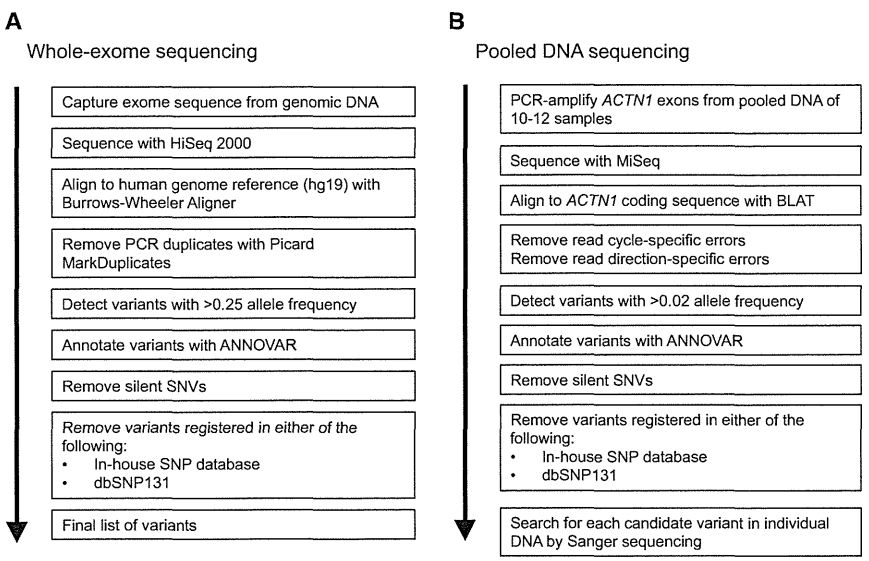


**Figure 1. A Flow Diagram of the Genomic Analysis**
(A) Detection of the candidate germline variants through Genomon-exome.[18]
(B) Screening of *ACTN1* variants with high-throughput sequencing of pooled DNA.[18]

(Illumina, San Diego, CA, USA). Candidate germline variants were detected through our in-house pipeline for exome-sequencing analysis with minor modifications for the detection of germline variants (Figure 1A).[18] The obtained sequences were aligned to the UCSC Genome Browser hg19 with the Burrows-Wheeler Aligner.[19] After removal of duplicate artifacts caused by PCR, the variants with an allele frequency > 0.25 were called. With a mean coverage of 117× (74×–176×), more than 92% of the 50 Mb target sequences were analyzed by greater than ten independent reads (Figure S2). In total, we identified 3,601 nucleotide variants that had not been registered in either the in-house SNP database or dbSNP131, and 360 of these cosegregated with macrothrombocytopenia in the corresponding families. The statistical analysis of the cosegregating variants indicated that only *ACTN1* (MIM 102575, RefSeq accession number NM_001102.3), which encodes α-actinin-1 (ACTN1), was found to be significantly mutated in our cohort (Table S1), for which variants c.313G>A (p.Val105Ile), c.94C>A (p.Gln32Lys), and c.2255G>A (p.Arg752Gln) were confirmed in pedigrees exome-1, exome-2, and exome-3, respectively (Figures 2A and 2B and Table 1). Sanger sequencing in the other seven dominant CMTP-affected pedigrees revealed an additional three variants, c.137G>A (p.Arg46Gln), c.2212C>T (p.Arg738Trp), and c.673G>A (p.Glu225Lys), which also cosegregated with macrothrombocytopenia within the individual pedigrees (Figures 2A and 2B and Table 1). Combined, cosegregating *ACTN1* variants were found in 6 (46%) out of 13 CMTP-affected pedigrees with a dominant mode of transmission ($p = 1.67 \times 10^{-6}$ compared to controls by a two-tailed Fisher's exact test). No *ACTN1* variants were detected among the 120 control individuals or 39 cases of sporadic CMTP, for which the mode of transmission had been unknown; the only exception was c.589C>T (p.Arg197Trp), which was found in a control individual who had a normal platelet count and size (Figure 1B and Figure S3). The multiple-sequence alignment indicated that all missense variants had highly conserved amino acid residues (Figure S4). Furthermore, different function-prediction programs suggested deleterious effects of these variants (Table S2). These results strongly suggest that these *ACTN1* variants represent autosomal-dominant CMTP-causing mutations.

Individuals with mutant *ACTN1* alleles had approximately half the normal platelet counts and a 30% increase in platelet size (Table 1 and Figure 3A). The platelet size in *ACTN1*-mutated individuals was smaller than that in individuals with a *MYH9* disorder or homozygous Bernard-Soulier syndrome but was similar to that in individuals with heterozygous Bernard-Soulier syndrome or GPIIb/IIIa-associated macrothrombocytopenia (data not shown). Electron microscopy showed no other abnormalities (Figure 3B). The macrothrombocytopenia was accompanied by anisocytosis. Bleeding diathesis was absent or mild if present: only two individuals (15%) experienced occasional epistaxis, and the bleeding time was within the normal limit (Table 1). In addition, no apparent in vitro defects in platelet functions, including normal platelet aggregation (Table 1), clot retraction, and platelet spreading on glass surfaces, were noted in *ACTN1*-mutated individuals (Figure S5). Flow cytometry showed increased expression of platelet GPIb/IX and GPIIb/IIIa, which were thought to reflect the increased platelet size (data not shown).

The affected protein, α-actinin, is a member of the actin-crosslinking protein superfamily that participates in the organization of the cytoskeleton.[20,21] Among the four known isoforms of α-actinin, *ACTN2* (MIM 102573) and *ACTN3* (MIM 102574) are relatively specific to muscle cells, whereas *ACTN1* and *ACTN4* (MIM 604638) are widely expressed in nonmuscle cells. Platelets and megakaryocytes mainly express *ACTN1* and, to a lesser extent, *ACTN4*.[22] The α-actinins exist as antiparallel dimers with an actin-binding domain (ABD) at the N terminus and cross-link actin filaments in bundles (Figure 2C). All of the identified *ACTN1* mutations reside within the functional domain (the ABD and the C-terminal calmodulin-like domain), but not within the spacer spectrin repeats (Figure 2D). Therefore, *ACTN1* variants that have differences in their structure and/or function might exert a dominant-negative effect, causing disorganization of actin filaments, although the localization and expression

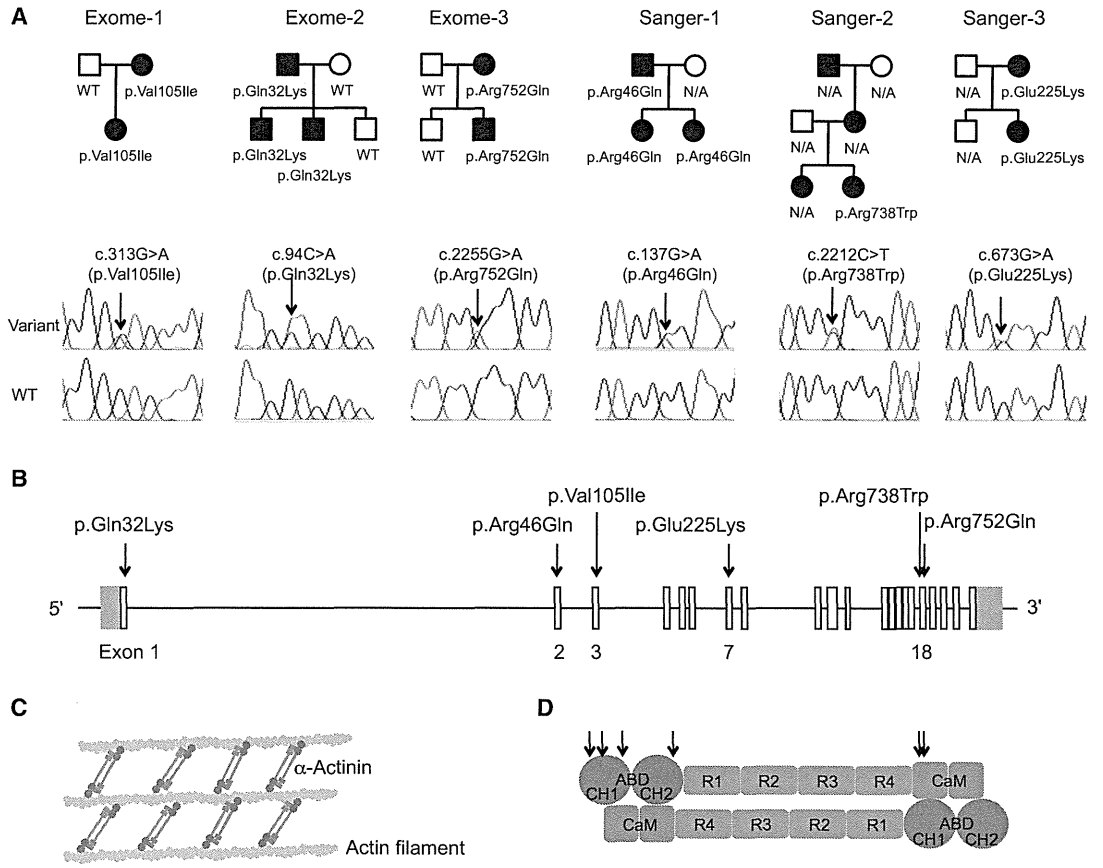


**Figure 2. Segregation of *ACTN1* Variants, the *ACTN1* Structure, α-Actinin-Actin Interaction, and the α-Actinin Domain Structure**
(A) The pedigrees for the six families affected by *ACTN1* variants are shown together with the Sanger-sequencing electropherograms. Filled symbols represent individuals affected by macrothrombocytopenia. The identified *ACTN1* variants are shown below the symbols. The arrows indicate nucleotide changes. The following abbreviations are used: WT, wild-type; and NA, not available.
(B) Genomic organization of *ACTN1*, variants in which are identified in individuals with CMTP.
(C) α-actinin cross-links actin filaments into actin-filament bundles.
(D) α-actinin consists of an N-terminal actin-binding domain (ABD), composed of two calponin homology domains (CHD), four spectrin repeats (R1–R4), and a C-terminal calmodulin-like domain (CaM). Two molecules form an antiparallel dimer. The arrows indicate the positions of the identified *ACTN1* variants.

of ACTN1 in the individuals' platelets was similar to that in controls (Figure S6). However, *ACTN4* missense mutations, which are implicated in familial focal segmental glomerulosclerosis (MIM 603278), promote the aggregation of α-actinin-4 molecules and abrogate the integrity of actin filaments in transfected cells.[23,24]

We therefore first evaluated the effects of mutant *ACTN1* on the organization of actin filaments by expressing each of the seven identified *ACTN1* variants in Chinese hamster ovary (CHO) cells. A full-length *ACTN1* sequence was amplified from normal platelet cDNA and constructed into mammalian expression vector pcDNA3.1 (Invitrogen, San Diego, CA, USA) with a 5′ Myc tag sequence. Six altered ACTN1 constructs (p.Gln32Lys, p.Arg46Gln, p.Val105Ile, p.Glu225Lys, p.Arg738Trp, and p.Arg752Gln) identified exclusively in the affected individuals and one construct (p.Arg197Trp) also identified in a control individual were prepared. Plasmid DNA was transfected into CHO cells with the PolyFect transfection reagent (QIAGEN, Hilden, Germany). Twenty-four hours after transfection, the ACTN1-transduced cells were replated on fibronectin (10 μg/ml)-coated coverslips for an immunofluorescence analysis.[16] As shown in Figure 4, cells transduced with wild-type ACTN1 showed well-organized, fine actin-filament networks, where ACTN1 colocalized in a large part onto the actin filaments, whereas unbound ACTN1 was finely distributed within the cytoplasm. In contrast, except for the p.Arg197Trp variant found in a control individual, all ACTN1 variants caused varying degrees of disorganization of the actin filaments in variant-transduced cells, in which ACTN1 colocalized with less fine, shortened actin filaments and in which unbound ACTN1 was coarsely distributed within the cytoplasm (some cells showed punctuated or condensed staining).

We further investigated whether altered ACTN1 also causes disorganization of the actin cytoskeleton in megakaryocytes by expressing wild-type and altered ACTN1 (p.Gln32Lys and p.Val105Ile) in primary mouse fetal liver-derived megakaryocytes by retrovirus-mediated gene transfer.[11] We subcloned wild-type and mutant *ACTN1*

**Table 1. *ACTN1* Mutations and Platelet Characteristics**

| Family | | DNA Mutation | Protein Alteration | Platelet Count ( × $10^9$/l) | Platelet Size (μm)[a] | Bleeding Tendency | Duke Bleeding Time (min) | Platelet Aggregation ADP (%) | Initial Diagnosis |
|---|---|---|---|---|---|---|---|---|---|
| Exome-1 | mother | c.313G>A | p.Val105Ile | 80 | 3.7 ± 1.1 | none | - | - | - |
| | proband | c.313G>A | p.Val105Ile | 91 | 3.8 ± 1.4 | none | - | - | immune thrombocytopenia |
| Exome-2 | father | c.94C>A | p.Gln32Lys | 113 | 2.7 ± 0.9 | none | - | - | congenital thrombocytopenia |
| | proband | c.94C>A | p.Gln32Lys | 54 | 3.1 ± 1.1 | none | 4.5 | 34 (2 μM) | congenital thrombocytopenia |
| | brother | c.94C>A | p.Gln32Lys | 124 | 2.9 ± 0.9 | epistaxis | - | - | congenital thrombocytopenia |
| Exome-3 | mother | c.2255G>A | p.Arg752Gln | 100 | ND | none | - | - | immune thrombocytopenia |
| | proband | c.2255G>A | p.Arg752Gln | 77 | 2.9 ± 0.6 | none | - | 49 (2 μM) | CMTP |
| Sanger-1 | father | c.137G>A | p.Arg46Gln | 131 | 4.2 ± 1.3 | none | 1 | 76 (2 μM) | - |
| | proband | c.137G>A | p.Arg46Gln | 120 | 3.9 ± 1.6 | none | - | 66 (2 μM) | CMTP |
| | sister | c.137G>A | p.Arg46Gln | 97 | 3.6 ± 1.4 | none | - | 74 (2 μM) | CMTP |
| Sanger-2 | proband | c.2212C>T | p.Arg738Trp | 77 | 3.7 ± 1.5 | none | 2 | - | CMTP |
| Sanger-3 | proband | c.673G>A | p.Glu225Lys | 80 | 3.0 ± 0.9 | epistaxis | - | 59 (2.5 μM) | CMTP |
| | mother | c.673G>A | p.Glu225Lys | 132 | 2.8 ± 0.8 | none | - | - | - |
| Mean ± SD | - | - | - | 98.1 ± 23.2 | 3.4 ± 0.5 | - | - | - | - |

The following abbreviations are used: ND, not done; and CMTP, congenital macrothrombocytopenia.
[a]Determined by a microscopic observation of 200 platelets on a stained peripheral-blood smear. Control size = 2.5 ± 0.3 μm (n = 31).

cDNAs into retroviral vector pGCDNsamIRES/EGFP with a 5′ Myc tag sequence and transfected them into 293 gpg packaging cells to obtain viral stocks.[25] We used the vesicular stomatitis virus G protein to pseudotype the envelope of the virus. Mouse fetal liver cells harvested from embryonic day 13.5 embryos were transduced with either vehicle vector or pGCDNsamIRES/EGFP ACTN1 and were cultured with 40 ng/ml recombinant mouse thrombopoietin. The Experimental Animal Committee of Nagoya Medical Center approved the animal studies.

On posttransduction day 3, large megakaryocytes were enriched with a 1.5/3% BSA gradient and were then incubated on fibrinogen-coated coverslips for 45 min in the presence of 100 nM phorbol myristate acetate.[26]

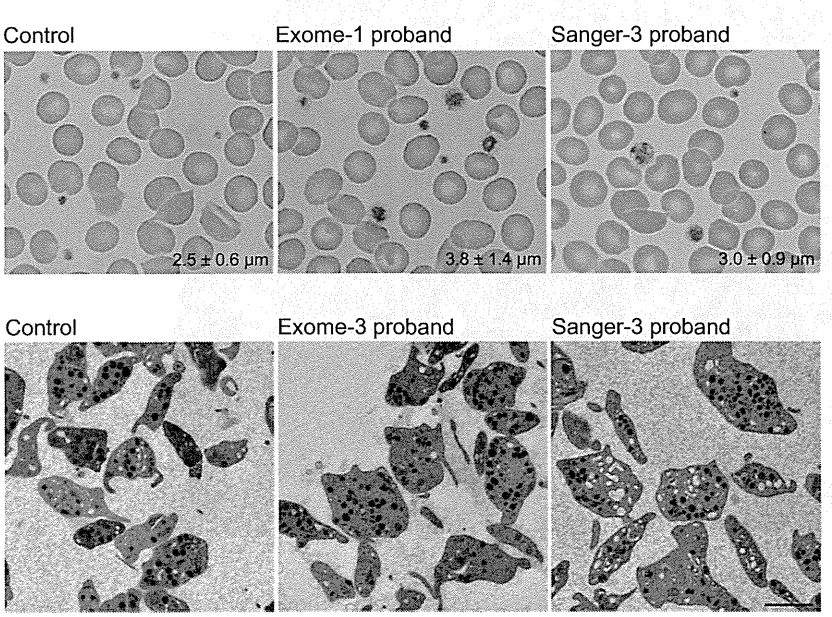


**Figure 3. The Platelet Morphology**
(A) Peripheral-blood smears were stained with May-Grünwald Giemsa for a normal control, the exome-1 proband, and the Sanger-3 proband. The affected individuals showed macrothrombocytopenia accompanied by anisocytosis. The number in each panel shows the mean platelet size (n = 200). Images were obtained with a BX50 microscope with a 100×/1.35 numeric aperture oil objective (Olympus, Tokyo, Japan). Images of the slides were acquired with a DP70 digital camera and DP manager software (Olympus). The original magnification is ×1,000.
(B) The ultrastructure of platelets from a normal control, the exome-3 proband, and the Sanger-3 proband. Platelet-rich plasma was prepared from acid-citrate-dextrose-citrated whole blood that was fixed in 2% glutaraldehyde and postfixed in 1% osmium tetroxide. The samples were then dehydrated in a graded ethanol series and n-butyl glycidyl ether and embedded in an epoxy resin (Epon 812; TAAB, Berkshire, UK). Ultrathin sections (0.1 μm) were doubly stained with 2% uranyl acetate and 1% lead citrate and were then observed with a transmission electron microscope (H-7650, Hitachi, Tokyo, Japan) at an accelerating voltage of 80 kV. The original magnification is ×1,500. The scale bar represents 2 μm.

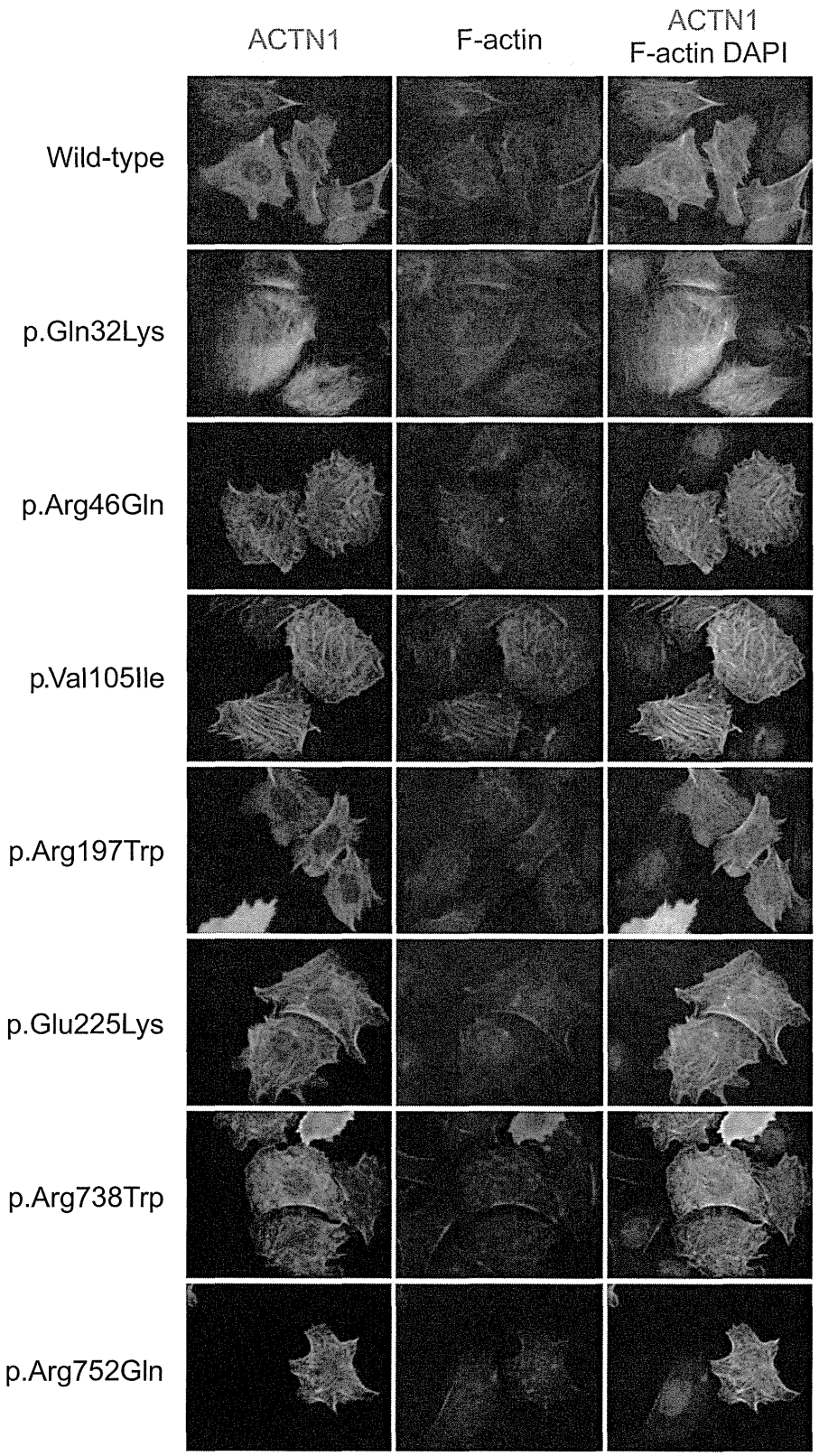


**Figure 4. The Subcellular Localization of Altered ACTN1 in CHO Cells**
CHO cells were transiently transfected with Myc-tagged wild-type or mutant *ACTN1* cDNAs. After the cells were replated on fibronectin-coated coverslips, they were fixed with 4% paraformaldehyde and permeabilized with 0.5% Triton X-100. They were then stained with Myc-tagged antibody (Invitrogen), followed by Alexa-488-labeled goat anti-mouse IgG, Alexa-555-conjugated phalloidin (Invitrogen), and DAPI. Images were obtained with a BX50 fluorescence microscope with a 40×/1.00 numerical aperture oil objective lens. The cells shown are representative of eight independent experiments.

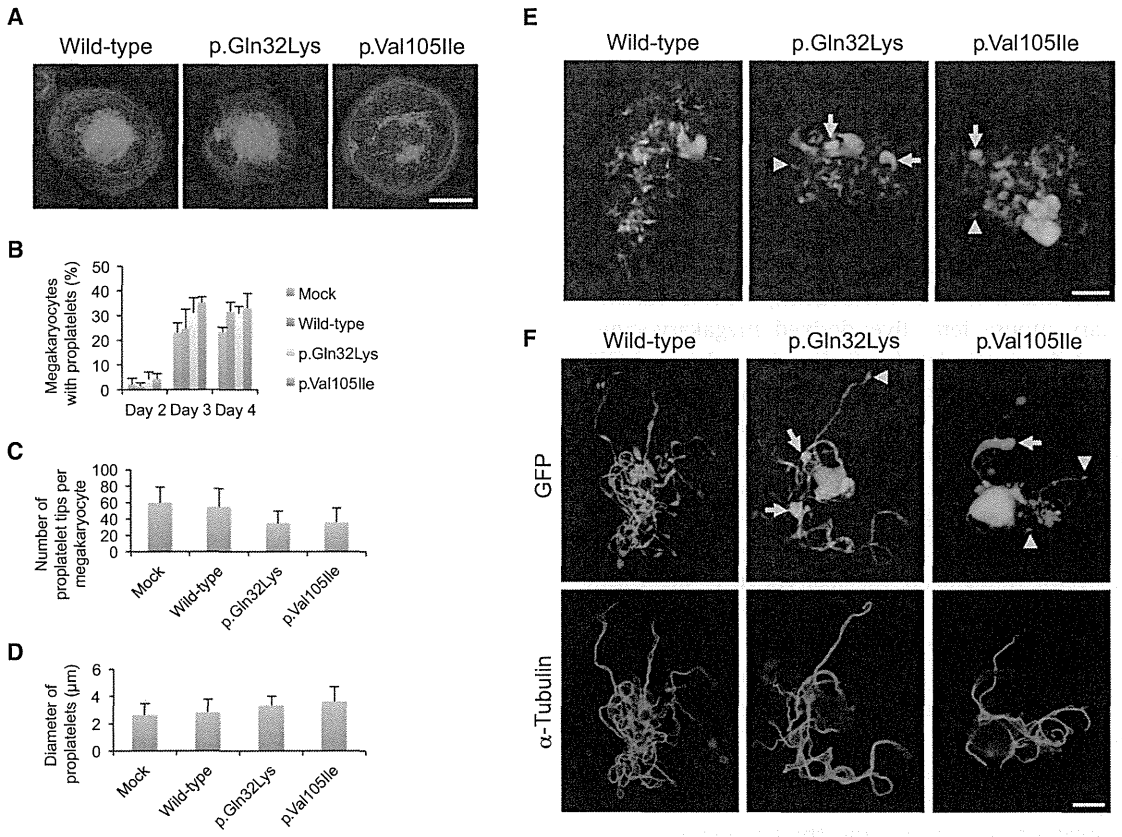


**Figure 5. Abnormal Proplatelet Formation in Megakaryocytes Transduced with Altered ACTN1**
(A) The organization of the actin filaments in megakaryocytes adhered to fibrinogen. The scale bar represents 50 μm.
(B) The percentage of megakaryocytes extending proplatelets was evaluated under an IX71 fluorescence microscope with a 20×/0.40 objective lens (Olympus) 2–4 days after infection. For each specimen, at least 100 megakaryocytes were evaluated.
(C) The number of proplatelet tips per megakaryocyte was decreased in megakaryocytes transduced with mutant *ACTN1*.
(D) The size of proplatelet tips was increased in megakaryocytes transduced with altered ACTN1.
(E) Representative megakaryocytes extending proplatelets 3 days after infection. Note that the size of the proplatelet tips was variable in the megakaryocytes transduced with altered ACTN1 (arrows indicate large tips, and arrowheads indicate small tips). The scale bar represents 50 μm.
(F) The proplatelet morphology and α-tubulin localization of EGFP-positive megakaryocytes. Infection day 3 cultures were cytospun onto glass slides. Cells were then fixed with 4% paraformaldehyde, permeabilized with 0.5% Triton X-100, and stained with GFP antibody (D153-3; Medical & Biological Laboratories, Nagoya, Japan) and α-tubulin antibody (RB-9281; Lab Vision, Fremont, CA), followed by Alexa-488-labeled goat anti-rat IgG and Alexa-555-labeled goat anti-rabbit IgG (Invitrogen). Images were obtained with a BX50 microscope with a 100×/1.35 numeric aperture oil objective lens (Olympus). The size of the proplatelet tips was variable in megakaryocytes transduced with altered ACTN1 (arrows indicate large tips, and arrowheads indicate small tips). The scale bar represents 20 μm. Representative images from four independent experiments are shown.

Cells were fixed, permeabilized, and stained with phalloidin, and then green-fluorescent-protein (GFP)-positive megakaryocytes were observed under a fluorescence microscope. Megakaryocytes adhere to fibrinogen-coated surfaces through the integrin αIIbβ3 receptor and undergo cytoskeletal reorganization. Cells transduced with wild-type ACTN1 reorganized the actin cytoskeleton with the development of organized actin filaments, which were circumferential and parallel to the cell periphery. However, the circumferential actin-filament network was less organized in the megakaryocytes transduced with altered ACTN1 than in control cells (Figure 5A). These findings indicate that CMTP-associated *ACTN1* mutations dominantly affect the actin-filament assembly and might result in abnormal cytoskeletal organization.

According to the current model of platelet production, differentiated megakaryocytes extend long, branching multiple microtubule-based protrusions, called proplatelets, into the bone-marrow sinusoids, which are composed of platelet-sized swellings, or tips, in tandem arrays that are mutually connected by thin cytoplasmic bridges.[27] Proplatelets are then released into the blood stream, where terminal production of mature platelets takes place through several intermediate forms.[28] The proplatelet formation and their release from megakaryocytes, as well as the subsequent production of mature platelets in the periphery, are spatially and temporally regulated by dynamic reorganization of the cytoskeletons and signal transduction.[29] Several lines of evidence suggest that macrothrombocytopenias are caused by defects in the

regulation of terminal platelet production.[30] In fact, most of the previously reported defects responsible for CMTP affect genes involved in the signaling pathways and/or components of the cytoskeleton;[30] these defects include mutations in integrin αIIbβ3 (*ITGA2B/ITGB3*),[11,12] GPIb/IX (*GP1BA*, *GP1BB*, and *GP9*),[5,6] nonmuscle myosin heavy chain IIA (*MYH9*),[4,5] actin-binding protein filamin A (*FLNA*),[9] and β1-tubulin (*TUBB1*).[16]

To further explore the effects of mutant *ACTN1* on proplatelet formation, after transducing ACTN1 variants into primary mouse fetal liver-derived megakaryocytes, we monitored proplatelet formation in enhanced-GFP (EGFP)-positive megakaryocytes in suspension by inverted fluorescence microscopy. The cultures were then spread onto glass slides and subsequently analyzed by immunofluorescence staining. During the 4 day culture period, the proportion of proplatelet-formation-positive megakaryocytes was not different among wild-type-, p.Gln32Lys-, and p.Val105Ile-transduced megakaryocytes, suggesting that ACTN1 variants do not accelerate or inhibit the rate of proplatelet formation and/or platelet production (Figure 5B). However, the number of proplatelet tips tended to be decreased, and the size of the tips increased in the megakaryocytes transduced with both altered forms of ACTN1 (Figures 5C and 5D).

During proplatelet formation, microtubules function to propel proplatelet elongation, and the actin cytoskeleton plays a critical role in bending and bifurcating the proplatelet shaft to increase the number of proplatelet tips. Cytochalasin-mediated inhibition of actin polymerization has been shown to interfere with proplatelet branching.[27] Moreover, mouse models for null alleles of actin-modulating genes, such as cofilin-1 (*Cfl1*), and a hypomorphic allele of WD repeat domain 1 (*Wdr1*) exhibit macrothrombocytopenia, indicating that dynamic changes in the actin cytoskeleton are required for normal platelet production.[31,32] Because ACTN1 plays a pivotal role in crosslinking actin filaments,[20,21] defective ACTN1 variants could cause deregulated actin-filament organization, as shown in CHO cells and cultured megakaryocytes (Figures 4 and 5A). Furthermore, we found that the platelet tips in wild-type-ACTN1-transduced megakaryocytes were uniform in size, whereas they were heterogeneous in the variant-transduced cells (Figures 5E and 5F). These results are consistent with the thrombocytopenia and increased platelet size (macrothrombocytopenia) accompanied by anisocytosis in the affected individuals, demonstrating that abnormal ACTN1 affects proplatelet formation.

In addition to playing a role in actin bundling, α-actinins have been shown to interact with a number of other cytoskeletal and receptor proteins.[20,21] In platelets, ACTN1 binds to β integrins and can mediate their signaling.[33] Thus, similar to the activating mutations in *ITGA2B/ITGB3*,[11,12] *ACTN1* mutations could also affect proplatelet formation through abnormal integrin signaling.

In summary, we identified *ACTN1* mutations that cause autosomal-dominant CMTP. In our cohort, *ACNT1* variants accounted for 5.5% of the dominant forms of CMTP cases, representing the fourth most common cause of Japanese CMTP. Our finding clearly demonstrates the effectiveness of whole-exome sequencing of CMTP-affected pedigrees for clarifying their genetic basis, although the limitation of the available pedigree samples for exome sequencing prevented further identification of the causative genes for the remaining families. Such studies also facilitate the differential diagnosis of congenital macrothrombocytopenia and can provide important information about the mechanisms of platelet production.

## Supplemental Data

Supplemental Data include six figures and two tables and can be found with this article online at http://www.cell.com/AJHG.

## Acknowledgments

This work was supported by Research on Measures for Intractable Diseases Project (H23-012), a matching fund subsidy from the Ministry of Health Labour and Welfare, the Japan Society for the Promotion of Science (Grant-in-Aid for Scientific Research 20591161 and 23591429), and the National Hospital Organization Research Fund (Network Research Grant for Congenital Thrombocytopenia). The supercomputing resources were provided by the Human Genome Center, the Institute of Medical Science, The University of Tokyo. We thank R.C. Mulligan for the 293 gp and 293 gpg cells, M. Onodera for pGCDNsamIRES/EGFP, K. Oguri and Y. Kusano for discussions on the expression analysis, and Y. Kito for technical assistance.

Received: October 6, 2012
Revised: December 20, 2012
Accepted: January 23, 2013
Published: February 21, 2013

## Web Resources

The URLs for the data presented herein are as follows:

Burrows-Wheeler Aligner, http://bio-bwa.sourceforge.net/index.shtml
ClustalW2 - Multiple Sequence Alignment, http://www.ebi.ac.uk/Tools/msa/clustalw2/
dbSNP, http://www.ncbi.nlm.nih.gov/projects/SNP/
Genomon-exome, http://genomon.hgc.jp/exome/en/index.html
Mutation Taster, http://www.mutationtaster.org/
Online Mendelian Inheritance in Man (OMIM), http://www.omim.org/
Picard, http://picard.sourceforge.net/
PolyPhen-2, http://genetics.bwh.harvard.edu/pph2
RefSeq, http://www.ncbi.nlm.nih.gov/RefSeq
SAMtools, http://samtools.sourceforge.net/
SIFT, http://sift.jcvi.org/
UCSC Genome Browser, http://genome.ucsc.edu/

## References

1. Balduini, C.L., and Savoia, A. (2012). Genetics of familial forms of thrombocytopenia. Hum. Genet. *131*, 1821–1832.

2. Kunishima, S., and Saito, H. (2006). Congenital macrothrombocytopenias. Blood Rev. *20*, 111–121.
3. Nurden, A.T., Freson, K., and Seligsohn, U. (2012). Inherited platelet disorders. Haemophilia *18*(*Suppl 4*), 154–160.
4. Kunishima, S., and Saito, H. (2010). Advances in the understanding of *MYH9* disorders. Curr. Opin. Hematol. *17*, 405–410.
5. Balduini, C.L., Pecci, A., and Savoia, A. (2011). Recent advances in the understanding and management of *MYH9*-related inherited thrombocytopenias. Br. J. Haematol. *154*, 161–174.
6. Kunishima, S., Kamiya, T., and Saito, H. (2002). Genetic abnormalities of Bernard-Soulier syndrome. Int. J. Hematol. *76*, 319–327.
7. Berndt, M.C., and Andrews, R.K. (2011). Bernard-Soulier syndrome. Haematologica *96*, 355–359.
8. Hart, A., Melet, F., Grossfeld, P., Chien, K., Jones, C., Tunnacliffe, A., Favier, R., and Bernstein, A. (2000). Fli-1 is required for murine vascular and megakaryocytic development and is hemizygously deleted in patients with thrombocytopenia. Immunity *13*, 167–177.
9. Nurden, P., Debili, N., Coupry, I., Bryckaert, M., Youlyouz-Marfak, I., Solé, G., Pons, A.C., Berrou, E., Adam, F., Kauskot, A., et al. (2011). Thrombocytopenia resulting from mutations in filamin A can be expressed as an isolated syndrome. Blood *118*, 5928–5937.
10. Nichols, K.E., Crispino, J.D., Poncz, M., White, J.G., Orkin, S.H., Maris, J.M., and Weiss, M.J. (2000). Familial dyserythropoietic anaemia and thrombocytopenia due to an inherited mutation in *GATA1*. Nat. Genet. *24*, 266–270.
11. Kunishima, S., Kashiwagi, H., Otsu, M., Takayama, N., Eto, K., Onodera, M., Miyajima, Y., Takamatsu, Y., Suzumiya, J., Matsubara, K., et al. (2011). Heterozygous *ITGA2B* R995W mutation inducing constitutive activation of the αIIbβ3 receptor affects proplatelet formation and causes congenital macrothrombocytopenia. Blood *117*, 5479–5484.
12. Nurden, A.T., Fiore, M., Nurden, P., and Pillois, X. (2011). Glanzmann thrombasthenia: A review of *ITGA2B* and *ITGB3* defects with emphasis on variants, phenotypic variability, and mouse models. Blood *118*, 5996–6005.
13. Kahr, W.H., Hinckley, J., Li, L., Schwertz, H., Christensen, H., Rowley, J.W., Pluthero, F.G., Urban, D., Fabbro, S., Nixon, B., et al. (2011). Mutations in *NBEAL2*, encoding a BEACH protein, cause gray platelet syndrome. Nat. Genet. *43*, 738–740.
14. Gunay-Aygun, M., Falik-Zaccai, T.C., Vilboux, T., Zivony-Elboum, Y., Gumruk, F., Cetin, M., Khayat, M., Boerkoel, C.F., Kfir, N., Huang, Y., et al. (2011). *NBEAL2* is mutated in gray platelet syndrome and is required for biogenesis of platelet α-granules. Nat. Genet. *43*, 732–734.
15. Albers, C.A., Cvejic, A., Favier, R., Bouwmans, E.E., Alessi, M.C., Bertone, P., Jordan, G., Kettleborough, R.N., Kiddle, G., Kostadima, M., et al. (2011). Exome sequencing identifies *NBEAL2* as the causative gene for gray platelet syndrome. Nat. Genet. *43*, 735–737.
16. Kunishima, S., Kobayashi, R., Itoh, T.J., Hamaguchi, M., and Saito, H. (2009). Mutation of the β1-tubulin gene associated with congenital macrothrombocytopenia affecting microtubule assembly. Blood *113*, 458–461.
17. Jackson, S.C., Sinclair, G.D., Cloutier, S., Duan, Z., Rand, M.L., and Poon, M.C. (2009). The Montreal platelet syndrome kindred has type 2B von Willebrand disease with the *VWF* V1316M mutation. Blood *113*, 3348–3351.
18. Yoshida, K., Sanada, M., Shiraishi, Y., Nowak, D., Nagata, Y., Yamamoto, R., Sato, Y., Sato-Otsubo, A., Kon, A., Nagasaki, M., et al. (2011). Frequent pathway mutations of splicing machinery in myelodysplasia. Nature *478*, 64–69.
19. Li, H., and Durbin, R. (2009). Fast and accurate short read alignment with Burrows-Wheeler transform. Bioinformatics *25*, 1754–1760.
20. Otey, C.A., and Carpen, O. (2004). α-actinin revisited: A fresh look at an old player. Cell Motil. Cytoskeleton *58*, 104–111.
21. Sjöblom, B., Salmazo, A., and Djinović-Carugo, K. (2008). α-actinin structure and regulation. Cell. Mol. Life Sci. *65*, 2688–2701.
22. Haudek, V.J., Slany, A., Gundacker, N.C., Wimmer, H., Drach, J., and Gerner, C. (2009). Proteome maps of the main human peripheral blood constituents. J. Proteome Res. *8*, 3834–3843.
23. Kaplan, J.M., Kim, S.H., North, K.N., Rennke, H., Correia, L.A., Tong, H.Q., Mathis, B.J., Rodríguez-Pérez, J.C., Allen, P.G., Beggs, A.H., and Pollak, M.R. (2000). Mutations in *ACTN4*, encoding α-actinin-4, cause familial focal segmental glomerulosclerosis. Nat. Genet. *24*, 251–256.
24. Yao, J., Le, T.C., Kos, C.H., Henderson, J.M., Allen, P.G., Denker, B.M., and Pollak, M.R. (2004). α-actinin-4-mediated FSGS: an inherited kidney disease caused by an aggregated and rapidly degraded cytoskeletal protein. PLoS Biol. *2*, e167.
25. Nabekura, T., Otsu, M., Nagasawa, T., Nakauchi, H., and Onodera, M. (2006). Potent vaccine therapy with dendritic cells genetically modified by the gene-silencing-resistant retroviral vector GCDNsap. Mol. Ther. *13*, 301–309.
26. Shiraga, M., Ritchie, A., Aidoudi, S., Baron, V., Wilcox, D., White, G., Ybarrondo, B., Murphy, G., Leavitt, A., and Shattil, S. (1999). Primary megakaryocytes reveal a role for transcription factor NF-E2 in integrin α IIb β 3 signaling. J. Cell Biol. *147*, 1419–1430.
27. Italiano, J.E., Jr., Lecine, P., Shivdasani, R.A., and Hartwig, J.H. (1999). Blood platelets are assembled principally at the ends of proplatelet processes produced by differentiated megakaryocytes. J. Cell Biol. *147*, 1299–1312.
28. Thon, J.N., Montalvo, A., Patel-Hett, S., Devine, M.T., Richardson, J.L., Ehrlicher, A., Larson, M.K., Hoffmeister, K., Hartwig, J.H., and Italiano, J.E., Jr. (2010). Cytoskeletal mechanics of proplatelet maturation and platelet release. J. Cell Biol. *191*, 861–874.
29. Hartwig, J.H., and Italiano, J.E., Jr. (2006). Cytoskeletal mechanisms for platelet production. Blood Cells Mol. Dis. *36*, 99–103.
30. Thon, J.N., and Italiano, J.E., Jr. (2012). Does size matter in platelet production? Blood *120*, 1552–1561.
31. Bender, M., Eckly, A., Hartwig, J.H., Elvers, M., Pleines, I., Gupta, S., Krohne, G., Jeanclos, E., Gohla, A., Gurniak, C., et al. (2010). ADF/n-cofilin-dependent actin turnover determines platelet formation and sizing. Blood *116*, 1767–1775.
32. Kile, B.T., Panopoulos, A.D., Stirzaker, R.A., Hacking, D.F., Tahtamouni, L.H., Willson, T.A., Mielke, L.A., Henley, K.J., Zhang, J.G., Wicks, I.P., et al. (2007). Mutations in the cofilin partner Aip1/Wdr1 cause autoinflammatory disease and macrothrombocytopenia. Blood *110*, 2371–2380.
33. Tadokoro, S., Nakazawa, T., Kamae, T., Kiyomizu, K., Kashiwagi, H., Honda, S., Kanakura, Y., and Tomiyama, Y. (2011). A potential role for α-actinin in inside-out αIIbβ3 signaling. Blood *117*, 250–258.

Ann Hematol (2013) 92:1–9
DOI 10.1007/s00277-012-1564-5

ORIGINAL ARTICLE

# Clinical and genetic characteristics of congenital sideroblastic anemia: comparison with myelodysplastic syndrome with ring sideroblast (MDS-RS)

**Rie Ohba · Kazumichi Furuyama · Kenichi Yoshida · Tohru Fujiwara · Noriko Fukuhara · Yasushi Onishi · Atsushi Manabe · Etsuro Ito · Keiya Ozawa · Seiji Kojima · Seishi Ogawa · Hideo Harigae**

Received: 30 May 2012 / Accepted: 21 August 2012 / Published online: 16 September 2012
© The Author(s) 2012. This article is published with open access at Springerlink.com

**Abstract** Sideroblastic anemia is characterized by anemia with the emergence of ring sideroblasts in the bone marrow. There are two forms of sideroblastic anemia, i.e., congenital sideroblastic anemia (CSA) and acquired sideroblastic anemia. In order to clarify the pathophysiology of sideroblastic anemia, a nationwide survey consisting of clinical and molecular genetic analysis was performed in Japan. As of January 31, 2012, data of 137 cases of sideroblastic anemia, including 72 cases of myelodysplastic syndrome (MDS)–refractory cytopenia with multilineage dysplasia (RCMD), 47 cases of MDS–refractory anemia with ring sideroblasts (RARS), and 18 cases of CSA, have been collected. Hemoglobin and MCV level in CSA are significantly lower than those of MDS, whereas serum iron level in CSA is significantly higher than those of MDS. Of 14 CSA for which DNA was available for genetic analysis, 10 cases were diagnosed as X-linked sideroblastic anemia due to *ALAS2* gene mutation. The mutation of *SF3B1* gene, which was frequently mutated in MDS-RS, was not detected in CSA patients. Together with the difference of clinical data, it is

**Electronic supplementary material** The online version of this article (doi:10.1007/s00277-012-1564-5) contains supplementary material, which is available to authorized users.

R. Ohba · T. Fujiwara · N. Fukuhara · Y. Onishi · H. Harigae (✉)
Department of Hematology and Rheumatology,
Tohoku University Graduate School of Medicine,
1-1 Seiryo-machi, Aoba-ku,
Sendai 980-8574, Japan
e-mail: harigae@med.tohoku.ac.jp

K. Furuyama
Department of Molecular Biology and Applied Physiology,
Tohoku University Graduate School of Medicine,
Sendai, Japan

K. Yoshida · S. Ogawa
Cancer Genomics Project, Graduate School of Medicine,
The University of Tokyo,
Tokyo, Japan

T. Fujiwara · H. Harigae
Department of Molecular Hematology/Oncology,
Tohoku University Graduate School of Medicine,
Sendai, Japan

A. Manabe
Department of Pediatrics, St Luke's International Hospital,
Hirosaki University Graduate School of Medicine,
Hirosaki, Japan

E. Ito
Department of Pediatrics,
Hirosaki University Graduate School of Medicine,
Hirosaki, Japan

K. Ozawa
Division of Hematology, Jichi Medical University,
Shimotsuke, Japan

S. Kojima
Department of Pediatrics,
Nagoya University Graduate School of Medicine,
Nagoya, Japan

suggested that genetic background, which is responsible for the development of CSA, is different from that of MDS-RS.

**Keywords** Congenital sideroblastic anemia · Myelodysplastic syndrome · ALAS2

## Introduction

Sideroblastic anemia is characterized by anemia with the emergence of ring sideroblasts in the bone marrow. Ring sideroblasts are formed by the irregular accumulation of iron in mitochondria. There are two forms of sideroblastic anemia i.e., congenital sideroblastic anemia (CSA) and acquired sideroblastic anemia. Most of acquired sideroblastic anemia cases were included in myelodysplastic syndrome (MDS). To date, mutations of genes involved in heme biosynthesis, Fe–S cluster biogenesis, or the biology of mitochondria have been reported in CSA [1–5]. Impaired function of these genes is speculated to result in disutilization of iron, leading to accumulation of iron in mitochondria. Acquired sideroblastic anemia in MDS is categorized either as refractory cytopenia with multilineage dysplasia (RCMD) or refractory anemia with ring sideroblasts (RARS) depending on the level of dysplasia. In contrast CSA, mechanism of forming ring sideroblasts in MDS is not clarified, although it was recently suggested that the mutations of splicing pathway are involved in the pathogenesis of MDS [6]. It is possible that there is a common mechanism between CSA and MDS; however, mutations in genes, which are responsible for development of the CSA, have not been identified in MDS.

The most common form of CSA is X-linked sideroblastic anemia (XLSA), which is caused by mutation of erythroid-specific 5-aminolevulinate synthase (*ALAS2*), the first enzyme of heme synthesis in erythroid cells [7–10]. More than half of the patients with XLSA respond to the administration of pyridoxine [vitamin B6 (Vit.B6)], or pyridoxal 5-phosphate (PLP), which is the coenzyme of *ALAS2* [11]. In XLSA, adult onset cases have been reported [12, 13]; therefore, it is possible that some cases of CSA may be misdiagnosed as MDS, especially RARS. However, the clinical and pathological features of congenital and acquired sideroblastic anemia have not been fully clarified because there have been no comprehensive studies, including clinical and genetic analyses, focusing on sideroblastic anemia.

Here, we performed a nationwide survey of sideroblastic anemia in Japan to investigate the epidemiology and pathogenesis of this disease. The difference of clinical data and results of genetic analysis suggest that genetic background, which is responsible for the development of CSA, is distinct from that of MDS-RS.

## Materials and methods

### Data acquisition

This study consisted of three investigations. First, patients with sideroblastic anemia were searched by questionnaire sent to hospitals with hematology department (493 hospitals) and pediatric hematology department (593 hospitals) asking for information about patients diagnosed as sideroblastic anemia (first investigation) over the past 10 years. Next, detailed clinical data of sideroblastic anemia patients were collected from the hospital based on responses to the first investigation (second investigation). Survey items were age of onset, gender, family history, hematological and biochemical findings, treatment, and cause of death. Then, genetic analysis of patients, who were diagnosed as CSA and MDS without chromosomal anomaly, was performed in cases for which genome sample was available (third investigation).

This study was approved by the ethics committee of Tohoku University Graduate School of Medicine, the center responsible for clinical and genetic analysis. Informed consent for the genetic analysis was obtained in all cases.

### Diagnostic procedure

Ring sideroblasts were defined following the 2001 World Health Organization (WHO) classification. Sideroblastic anemia patients were diagnosed in the respective institutions. In all cases, bone marrow smears were investigated, and at least 15 % ring sideroblasts were confirmed by iron staining. Furthermore, diagnosis for RARS was made when dysplasia restricted to erythroid lineage in bone marrow was recognized. Diagnosis for RCMD was made when there is multilineage dysplasia. Thereafter, in the present study, RCMD correspond to refractory cytopenia with multilineage dysplasia and ringed sideroblasts (RCMD-RS) of the 2001 WHO classification. Diagnosis for CSA was made when the patient had a family history or the disease onset during infancy, or fulfilled the characteristic features of XLSA, such as onset at a young age, microcytic anemia, and responsiveness to Vit.B6.

### Genetic analysis of patients with sideroblastic anemia

In the genetic analysis, mutations in *ALAS2*, *SLC25A38*, *GLRX5*, *ABCB7*, *PUS1*, and *SLC19A2,* which are known to be responsible for CSA, were examined in 14 cases of CSA and 10 cases of MDS. In addition, *SF3B1*, which was very recently reported to be mutated in sideroblastic anemia in MDS at a high incidence, were analyzed as well. Mutation analysis for the *ALAS2* gene was performed first in all candidates, and then the analysis proceeded to the other

genes if no mutations in *ALAS2* were detected. For mutation analysis of *ALAS2*, genomic DNA was extracted from the proband's peripheral blood using QIAamp DNA blood midi kit (QIAGEN, Valencia, CA, USA). The proximal promoter region [14], erythroid enhancer in intron 8 [15], and all exons and exon–intron boundaries of the *ALAS2* gene were amplified using ExTaq DNA polymerase (Takara Bio, Shiga, Japan) [16]. Amplified products were purified using a QIAquick gel extraction kit (QIAGEN) after agarose gel electrophoresis. They were then subjected to direct sequencing analysis using BigDye Terminator Cycle sequencing kit v1.1 with an ABI3100 genetic analyzer (Life Technologies Corp., Carlsbad, CA, USA). Mutation of the gene was confirmed by repeated polymerase chain reaction (PCR) followed by direct sequencing analysis. Genes other than *ALAS2* were sequenced by Hiseq2000® [6]. Briefly, genomic DNA was amplified using REPLI-g mini kit® (QIAGEN Science). After adjusting the concentration of amplified DNA, DNA from consecutive 12 samples was combined into one DNA pool, and the entire coding sequences were amplified by primers to which *Not*I linker was attached. The products were digested with *Not*I, and ligated with T4 ligase. Then, DNA was sonicated into ~200-bp fragments, and sequencing libraries were generated. Libraries were subjected to deep sequencing on Hiseq2000®. Sequencing data was analyzes as described previously. Detected mutations were validated by direct sequence.

### Analysis of enzymatic activity of recombinant ALAS2 protein

For preparing recombinant ALAS2 proteins, complementary DNA (cDNA) encoding mature human ALAS2 protein was amplified using a following primer set (5′-GGTGGTCATATGATCCACCTTAAGGCAACAAAGG-3′and 5′-GGCATAGGTGGTGACATACTG-3′). The amplified cDNA was then treated with *Nde*I restriction enzyme and was cloned between *Nde*I and blunt-ended *Sap*I site of pTXB1 plasmid (New England Biolabs, Ipswich, MA, USA), resulting in pTXB-AEm. From this plasmid, mature ALAS2 protein was expressed as an inducible fusion protein with Intein and chitin-binding domain in *E. coli*. To obtain the mutant protein, the identified mutation was introduced into pTXB-AEm using PrimeStar Max site-directed mutagenesis kit (Takara Bio, Shiga, Japan). For expression and purification of wild-type and mutant ALAS2 proteins, *E. coli* BL21 (DE3) was transformed with each plasmid. The induction and purification of the recombinant proteins were performed using Impact system (New England Biolabs) according to manufacturer's instruction. Briefly, each recombinant protein was induced in *E. coli* with 0.1 mM IPTG at 25 °C for overnight. Then, cells were resuspended with lysis buffer (20 mM Tris–HCl pH8.5, 500 mM NaCl, 1 mM EDTA, 0.1 % Triton X-100, 1 mM PMSF, 1 μg/ml of antipain, pepstatin, and leupeptin). After the sonication and centrifugation, cleared cell lysates were incubated with chitin beads for 1 h at 4 °C, then washed with wash buffer (20 mM Tris–HCl pH8.5, 500 mM NaCl, 1 mM EDTA, and 0.1 % Triton X-100). Tag-free recombinant mature ALAS2 protein was obtained by on-column cleavage with 50 mM DTT in wash buffer at room temperature for 16 h. After the elution from the column, protein concentration was determined using Bio-Rad Protein assay reagent (Bio-Rad Laboratories, Inc., Hercules, CA, USA). The ALAS activity of each recombinant protein was measured in vitro, as described previously [8].

### Statistical analysis

Results are presented as means±SD with the exception of the age of onset, which is expressed as the median. Statistical analysis was performed using Student's *t* test, and $P<0.05$ was taken to indicate statistical significance.

## Results

### Epidemiology of sideroblastic anemia

As of 31 January 2012, detailed data for 148 sideroblastic anemia, including MDS and secondary sideroblastic anemia, patients have been collected. Excluding 10 cases of refractory anemia with excess blasts (RAEB) and one case of sideroblastic anemia due to alcohol, the remaining 137 cases were classified as 18 cases of CSA, 47 cases of RARS, and 72 cases of RCMD. Of 18 CSA cases, 7 were already confirmed to be XLSA due to mutation of *ALAS2* before registration in this study, and the others were diagnosed as CSA based on family history or clinical findings, including responsiveness to Vit.B6 treatment. Clinical findings and family history, which suggest the porphyria, were not observed in any CSA patients.

### Analysis of the pathology of congenital sideroblastic anemia

Laboratory data of CSA, RARS, and RCMD are shown in Tables 1 and 2. Median age at onset of CSA was younger than those of RARS and RCMD (19, 72.5, and 71 years old, respectively). Hemoglobin and mean corpuscular volume (MCV) values of CSA were significantly lower than those of RARS and RCMD cases (7.1 g/dl and 69.0 fl, 8.7 g/dl and 106.8 fl; and 8.3 g/dl and 106.5 fl, respectively). Serum iron level in CSA was significantly higher than that in RARS or RCMD (210.7, 162.8, and 171.1 μg/dl, respectively). These data have possibilities of reflecting the states of the iron over-loaded of CSA; however, as serum iron concentration is very instable and depends from different factors, this finding should be carefully evaluated.

**Table 1** Clinical data of CSA, RARS, and RCMD (1)

| | CSA ($n$=18) | RARS ($n$=47) | RCMD ($n$=72) | $p$-value (between CSA and RARS) | $p$-value (between CSA and RCMD) |
|---|---|---|---|---|---|
| Gender | | | | | |
| Male | 17 | 33 | 44 | | |
| Female | 1 | 14 | 28 | | |
| Median age at onset (year) | 19.0 (±20.2) | 72.5 (±10.4) | 71.0 (±13.0) | <0.01 | <0.01 |
| White blood cells (/μl) | 5547 (±2022) | 4741 (±2561) | 4105 (±1847) | 0.24 | <0.01 |
| Red blood cells ($\times 10^4$/μl) | 383.4 (±100.0) | 245.6 (±45.6) | 239.4 (±56.4) | <0.01 | <0.01 |
| Hemoglobin (g/dl) | 7.1 (±2.21) | 8.7 (±1.7) | 8.3 (±1.8) | <0.01 | 0.02 |
| Mean corpuscular volume (fl) | 69.0 (±11.6) | 106.8 (±9.0) | 106.5 (±9.2) | <0.01 | <0.01 |
| Platelet ($\times 10^4$/μl) | 28.5 (±12.62) | 25.9 (±15.5) | 23.9 (±24.1) | 0.53 | 0.44 |
| Reticulocyte (‰) | 12.1 (±10.9) | 17.7 (±10.8) | 21.5 (±20.1) | 0.07 | 0.05 |

When iron-related laboratory data were examined in transfusion independent cases (CSA, 13; RARS, 26; RCMD, 34), Serum iron level in CSA was tended to be higher than that in RARS or RCMD (210.6, 180.3, and 166.6 μg/dl, respectively), although the difference was not significant ($p$=0.07, data not shown). Serum ferritin level in CSA, RARS and RCMD were elevated in these transfusion independent cases (1,087.9, 898.1, and 732.2 ng/ml, respectively), suggesting that most of sideroblastic anemia patients were iron-overloaded before transfusion. There were no significant differences in other biochemical data among the three groups.

## Chromosomal abnormalities of MDS

Data regarding cytogenetic abnormalities were available for all RARS patients and for 68 of 72 RCMD patients. Figure 1 shows the cytogenetic findings of RARS and RCMD. In RARS cases, chromosomal abnormalities were found in 17 patients (36.2 %). Abnormalities consisted of abnormality including +8 (3 cases), complex abnormality with deletion 5 (2 cases), and complex abnormality with 20q− (3 cases). Chromosomal abnormalities in RCMD were found in bone marrow samples from 27 RCMD patients (39.7 %). Abnormality including +8 was detected in nine cases (33.3 %) and abnormality of idic (X) (q13), associated with the *ABCB7* gene [17], was found in one case. In addition, −7, which was not identified in RARS, was identified in four RCMD patients (14.8 %).

## Treatment and outcome

Analysis of the available data regarding treatment indicated that 17 of 47 RARS cases and 26 of 72 RCMD cases were administered Vit.B6 (data not shown). The effectiveness was judged according to the criteria of IWG [18], and one RARS patient obtained a major response, and three RARS patients and one RCMD patient obtained minor responses. Thus, 4 of 17 RARS patients and 1 of 26 RCMD patients responded to Vit.B6 treatment. However, improvement of Hb was not sustained in two RARS patients; Hb level gradually returned to or dropped below the pretreatment level. Therefore, Vit.B6 treatment may not be effective for MDS, or the effect if any may be very limited. The clinical outcomes of patients are shown in Supplemental Table 1. The median follow-up from the time of diagnosis in CSA patients was 30.5 months, and two patients died due to sepsis (one case) and cardiac failure (one case). One patient

**Table 2** Clinical data of CSA, RARS, and RCMD (2)

| | CSA ($n$=18) | RARS ($n$=47) | RCMD ($n$=72) | $p$-value (between CSA and RARS) | $p$-value (between CSA and RCMD) |
|---|---|---|---|---|---|
| Total bilirubin (mg/dl) | 1.1 (±0.8) | 1.3 (±0.9) | 1.1 (±0.7) | 0.47 | 0.78 |
| AST (GOT) (IU/l) | 33.0 (±24.3) | 24.9 (±11.7) | 27.9 (±20.8) | 0.08 | 0.38 |
| LDH (IU/l) | 218.3 (±98.9) | 263.5 (±119.2) | 246.1 (±97.7) | 0.16 | 0.28 |
| CRP (mg/dl) | 0.13 (±0.15) | 0.40 (±1.16) | 1.17 (±3.81) | 0.37 | 0.30 |
| Serum iron (mg/dl) | 210.7 (±77.6) | 162.8 (±73.6) | 171.1 (±66.2) | 0.03 | 0.04 |
| UIBC (mg/dl) | 80.4 (±113.6) | 102.4 (±82.7) | 79.9 (±60.7) | 0.48 | 0.93 |
| Ferritin (ng/ml) | 1239.8 (±1306.8) | 743.4 (±815.3) | 804.3 (±990.2) | 0.08 | 0.13 |